NASA Reference Publication 1378

NASA-RP-1378 19960008175

Magnetosphere Imager Science Definition Team Interim Report

T.P. Armstrong and C.L. Johnson

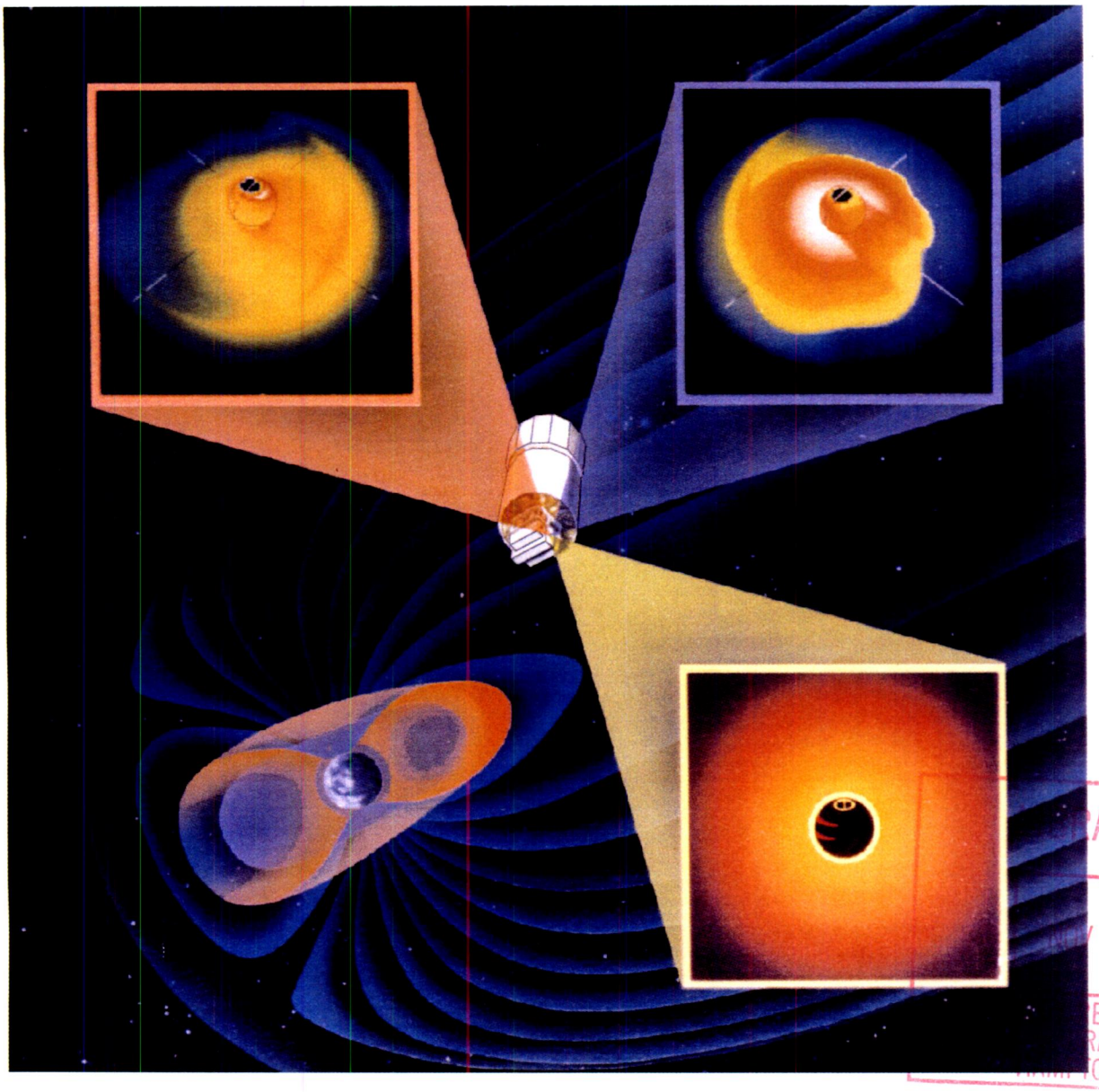

September 1995

NASA Reference Publication 1378

Magnetosphere Imager Science Definition Team Interim Report

T.P. Armstrong
University of Kansas, Lawrence, Kansas

C.L. Johnson
Marshall Space Flight Center • MSFC, Alabama

National Aeronautics and Space Administration
Marshall Space Flight Center • MSFC, Alabama 35812

September 1995

PREFACE

Many people contributed information and insights to this report, most of who are given credit. However, all members of the magnetosphere imager team were inspired by the energy, enthusiasm, kindness, and concern of Dr. Stanley Shawhan, whose death deprived the Space Physics Division of its first Director and all of us of a dear friend.

TABLE OF CONTENTS

TABLE OF CONTENTS

LIST OF ILLUSTRATIONS

LIST OF TABLES

REFERENCE PUBLICATION

MAGNETOSPHERE IMAGER SCIENCE DEFINITION TEAM INTERIM REPORT

INTRODUCTION

This report is the culmination of a process begun in 1989 when the Space Physics Division initiated a study of its present and future program, especially of missions that call for important commitments of resources to flight investigations. This study was a component of an Office of Space Science and Applications (OSSA)-wide evaluation of its science program. The work of the scientific community in defining the magnetosphere imager (MI) has proceeded in several phases alongside an evolving NASA concept of streamlining and expediting the conduct of its flight investigations. This report presents a scientific rationale and technical approach that is tailored to the present NASA tactical approach of using focused, cost-constrained, timely, and "small" (just large enough to do the job) missions. In order to achieve this focus, the MI Science Definition Team (SDT) first considered the state of magnetospheric knowledge and what important questions needed to be resolved by magnetospheric imagery. Then the SDT identified "core" scientific objectives and the measurements required for their attainment. Both large and small spacecraft approaches were considered. The final spacecraft, instrumentation, and mission concepts represent the SDT's judgment on the minimum resources required to attain the MI science objectives.

The SDT was constituted by the division in 1991 after the objectives of magnetospheric imaging had emerged from the 1989 to 1990 studies as having high merit and needing to be examined in some depth. The SDT was selected from among those scientists whose published work and experience applies to magnetospheric emissions and to the imagery derived therefrom. Responsibility for studying the mission concept and its implementation was assigned to the Marshall Space Flight Center (MSFC).

As initially conceived in 1991, the MI was to be accomplished via a then "intermediate" program costing about $230M and using a Delta-class launcher and a 1,200-kg spacecraft.

As budgetary constraints on new missions became more severe in 1991 and 1992, the SDT and MSFC program development team examined a much smaller spacecraft concept, around 400 kg and without a despun and pointed platform. This approach consolidated the functions of the auroral and geocoronal imagers and used a spin-scan imaging technique to avoid the expense of a pointed platform. The complexity and size of the spacecraft and its instruments was reduced to $120M through these changes. Further reduction of spacecraft capability and simplifications of the program allowed estimated costs of less than $100M. These cost figures are presented here not as final and authoritative, but for their information value in understanding how the spacecraft and mission concepts presented here have arrived at their present characteristics.

MEMBERSHIP OF THE MI SCIENCE DEFINITION TEAM

Thomas P. Armstrong (Chairman)	University of Kansas
A. Lyle Broadfoot	University of Arizona
Supryia Chakrabarti	Boston University
Louis A. Frank	University of Iowa
Dennis L. Gallagher (Study Scientist)	NASA Marshall Space Flight Center
James L. Green	NASA Goddard Space Flight Center
Ke Chiang Hsieh	University of Arizona
Barry H. Mauk	Johns Hopkins University Applied Physics Laboratory
David J. McComas	Los Alamos National Laboratory
Robert R. Meier	Naval Research Laboratory
Steven B. Mende	Lockheed Missiles and Space Corporation
Thomas E. Moore	NASA Marshall Space Flight Center
George K. Parks	University of Washington
Edmund C. Roelof	Johns Hopkins University Applied Physics Laboratory
Mark F. Smith	NASA Goddard Space Flight Center
Jan Sojka	Utah State University
Donald J. Williams	Johns Hopkins University Applied Physics Laboratory

MEMBERSHIP OF THE RADIO PLASMA SOUNDER TEAM

The Space Physics Division convened an ad hoc panel to evaluate the scientific feasibility and potential return from a radio plasma sounding (RPS) investigation of the magnetosphere. This possibility arose via suggestions that RPS might provide a valuable enhancement to MI science. This team has met and provided its own report. However, highlights of their findings are included here under the category of potential scientific enhancements.

James L. Green (Chair)	NASA Goddard Space Flight Center
Robert F. Benson	NASA Goddard Space Flight Center
Wynne Calvert	University of Iowa
Donald Carpenter	Stanford University
Shing Fung	NASA Goddard Space Flight Center
Patricia Reiff	Rice University
Bodo Reinisch	University of Massachusetts, Lowell
William Taylor	Nichols Research Corporation
	Liaisons
Dennis L. Gallagher	NASA Marshall Space Flight Center
Mark F. Smith	NASA Goddard Space Flight Center

MEMBERSHIP OF THE MSFC PRELIMINARY DESIGN TEAM

Carmine DeSanctis	Director, Advanced Systems and Technology Office
Les Johnson	Study Manager
Melody Herrmann	Lead Engineer
Reggie Alexander	Thermal Control
Harold Blevins	Communications
Tom Buzbee	Conceptual Art
Connie Carrington	Guidance and Control
Holly Chandler	Mass Analysis
Greg Hajos	Configuration and Layout
George Kearns	Propulsion
Larry Kos	Orbit Analysis
Lou Maus	Power
Andy Prince	Cost Analysis
Terri Schmitt	Launch Vehicles
Susan Spencer	Structures

SCIENCE OBJECTIVES

Science Objectives

Global Picture
To observe and interpret the global shape of the inner magnetosphere using simultaneous images of the ring current, inner plasma sheet, plasmasphere, aurora, and geocorona.

Global Response
To understand how magnetospheric current systems, fields, and conductivities respond to internal and external influences.

Global Mapping
To visualize and identify the connections of various magnetospheric components to each other, especially as these connections act to change the components during substorms and solar wind variations.

Global Framework
To relate global images of the magnetosphere to local observations in order to
(a) Learn how local processes combine to form the whole
(b) Provide a global framework within which to place local observations
(c) Provide a "ground-truth" for the global observations

Features and Emissions Observed

The ring current and inner plasmasheet
Energetic neutral atoms (ENA) resulting from charge exchange between plasma and neutral, geocoronal hydrogen will image the structure of the ring current (20 to 200 keV H^+ and O^+, suprathermal plasma) the inner plasmasheet (1 to 10 keV H^+ and O^+, thermal plasma).

The plasmasphere
Extreme ultraviolet (EUV) photons resulting from 30.4 nm sunlight resonantly scattered by He^+ will image the structure of the cold (10^3 to 10^4 K) plasmasphere.

The electron and proton aurorae
Far ultraviolet (FUV) photons emitted by oxygen (130.4 nm and 135.6 nm), and N_2 molecules (LBH bands at 127.3 nm, 132.5 nm, 135.4 nm, and 138.4 nm) will image the electron aurora.

The geocorona
FUV photons resulting from 121.6 nm sunlight resonantly scattered from neutral H will image the structure of the geocorona.

OPPORTUNITIES FOR PUBLIC EDUCATION

NASA has recognized the desirability of making educational outreach a critical aspect of all future space missions. In particular, in NASA's Strategic Plan for Space Sciences (1994) it is stated that:

> "We will use NASA's mission, unique facilities, and specialized workforce to promote excellence in America's educational system. Specifically, we will work to enhance scientific and technical competence and literacy. We will do this by capturing the educational potential of each NASA program and by conducting and facilitating education programs at all educational levels."

The MI mission is uniquely suitable for educational outreach activities. Because the MI data products are images of nature, their accessibility and information value to the general public will be very high. Images allow scientists to interact with the general public in ways not possible with equations, words, or numbers. School children and taxi drivers will form impressions of, and curiosity about, the MI products. With suitable use of communications and widely available image distribution technologies, MI products will be available, for example, to nightly news presentations. Such space weather concepts as the magnetospheric and terrestrial responses to large solar and interplanetary disturbances can be vividly and promptly illustrated for the public.

In parallel with the recent recognition of the importance of educational outreach activities within NASA has been the much broader consideration by numerous national associations of science educational reform and of the development of national science educational standards (e.g., AAAS, NRC). In the kindergarten through 12th grade educational arena, the importance of in-class activities has been emphasized. To be effective in educational outreach, NASA project personnel must participate, along with educational professionals, in the development of curriculum materials for in-class use and participate in teacher training activities so that the in-class materials can be competently utilized. The materials (among other characteristics) must be hands-on, be developmentally appropriate, be inquiry-based with students as researchers, allow for indepth examination of a topic, and utilize a range of classroom technologies.

The MI data are image based, and yet the images relate to quantitative concepts that can connect to a student's own experiences. As described above, the images make the natural space environment extremely accessible to students. On a quantitative basis, the first level task of interpreting the images is to relate the image pixel intensities to the densities and temperatures of the plasma "gases." Such concepts are easy to understand based on the student's own experiences and science studies of atmospheric and other gases here on the surface of the Earth. A similar connection is made when the near-Earth environment is presented as the extension of the Earth's atmospheric system. This will be particularly clear when the variations in the images are presented in the context of "space weather" where the analogy with the weather associated with the atmospheric gases close to the Earth can be made obvious to the student.

Because the MI data are image based, allowing for easy accessibility to complex natural phenomena, and because the quantitative aspects can be related to concepts with which the students are well familiar, the MI data will be especially suitable for the generation of in-class, inquiry-based, curriculum units that are suitable for kindergarten through 12th grade educational activities.

Because of the accessibility of image data, it is anticipated that the MI educational approach will contribute to a broad spectrum of educational and public forums. In the same way that the most fundamental concepts of our local plasma environment will be illustrated for kindergarten through 12th grade students, the more sophisticated concepts of electric and magnetic fields and of charged particle motions will be vividly portrayed for students at the college and graduate school levels. Students, educators, and researchers whose interests include such subjects as space environment-induced errors in radio frequency navigational systems, engineering designs and operational plans for space-based communication satellites, and the fault tolerance of ground power distribution grids will benefit from the image and image-derived products of the MI mission.

The rapid growth of information technologies in combination with the more traditional settings of museums, science centers, and libraries will offer a rich spectrum of opportunities for the public to become aware of the importance and character of our local plasma environment through the MI mission. Television and now the Nation's Information Superhighway (the Internet) are rapidly becoming dominant sources of information in people's homes. The World Wide Web, through software products such as MOSAIC™, has lead to an explosion of public access to digital information in the form of images, documents, sound, and motion video. An Internet-based MI MOSAIC™ home page containing mission news and data products, along with the classroom activities described above, will certainly be a part of the MI mission.

MI MISSION CONCEPT AND ANTICIPATED RESULTS

Mission Concept

Spacecraft
413 kg, 1.5- by 1.3-m. spinner
(includes 30-percent contingency)
accommodates 3 core instruments (plus
1 to 2 enhancing instruments)
40-kb/s data rate
24-min downlink per orbit

Launcher
Enhanced Taurus, Conestoga, or LLV
capability

Orbit
4,800-km by 7-R_E altitude
90° inclination
15.16-h period
Final Apogee at 49° North

Instruments
Hot Plasma Imager, Full sky,
1 image/minute,
hydrogen and oxygen ENA, 1 to 50 keV
(3° resolution) and 20 to 1,000 keV (2°
resolution)

Plasmasphere Imager, Full sky, 0.5°
resolution, 1 image/minute, 30.4 nm
sunlight resonantly scattered from He^+

Far Ultraviolet Imager, 40° by 360°, 0.1°
resolution, 1 image/minute

Anticipated Results

The first simultaneous images of the ring current, plasmasphere, aurora, and geocorona will be obtained.

The instantaneous shape of major magnetospheric features will be available to compare with theoretical models and with shapes inferred from in situ measurements.

Images of the global changes in the ring current, aurorae, and plasmasphere during magnetospheric substorms will reveal the strength and nature of the connections between these elements of the terrestrial system.

The global response of the magnetosphere to solar and interplanetary disturbances will be revealed.

The spatial patterns of injection and decay of hot plasma in the ring current and of the accompanying aurorae will reveal the sources of plasma and its consequences.

The transport of plasmaspheric He^+ and formation of the plasmapause will reveal global patterns of convection electric fields and relationship to ionospheric outflow.

MEASUREMENT PARAMETERS

The SDT concludes that the MI scientific objectives can be met by observations having the minimum characteristics given in the following. These characteristics are achievable within the currently available technologies that can be qualified for flight. Further, this instrumentation does not require exceptional spacecraft accommodations.

Instrument	Energetic Neutral Atoms ENA Imager	Plasmasphere Imager	FUV Imager	
Region	Ring current and inner plasma sheet	Plasmasphere	Aurora	Geocorona
Time Resolution (Images/minute)	1	1	1	1
Angular Resolution	High: 2° Low: 3°	0.5°	0.1°	1°
Emission Detected	Charge exchange with neutrals: hydrogen, helium, and oxygen	Sunlight resonantly reradiated from singly ionized helium	Emissions from atmospheric H, O, and N_2	Sunlight scattered from neutral hydrogen
Spectral Passbands	Low: $1 < E < 50$ keV High: $20 < E < 1{,}000$ keV $0.2 < DE/E < 0.4$	$\lambda = 30.4$ nm, He^+ Full integration of isolated line	$\lambda = 120$ to 190 nm $\Delta\lambda = 3.0$ nm	$\lambda = 121.6$ nm, Lyα $\Delta\lambda = 3.0$ nm
Field of View	4π	4π	40° by 40°	40° by 360°
Pixels/Image	90 by 180	180 by 360	400 by 400	40 by 360
Parameters Derived	Spatial, spectral, and compositional distributions of hot plasmas and energetic particle intensities	Spatial distribution of cold plasma density	Morphology of electron precipitation	Neutral atomic hydrogen density.
Features Resolved	0.2 R_E (Apogee)	0.1 R_E	80 km	1.0 R_E
Threshold Sensitivity	1 ENA /cm^2/s/ster/keV	0.1 Rayleighs	200 Rayleighs	10 Rayleighs

MI SCIENTIFIC RATIONALE

The Quest for a Global Magnetospheric View

The Beginnings: Thirty-six years ago, James A. Van Allen and his colleagues forever changed our popular view of near-Earth space as a bland and empty void. Using instruments onboard the first NASA satellite, Explorer 1, they discovered an unexpected and teeming population of charged particles confined within the Earth's magnetic field. Immediately following this discovery, global models of these trapped particles—the Van Allen radiation belts—were developed from their theoretically expected motions in the Earth's field as it was known at the time. This desire to build a global picture based on the few available measurements in the Earth's space environment has proven prophetic. From these earliest days one of the major quests of space plasma physics has been to develop an accurate global perspective of the magnetosphere and of its component parts.

Over the past three-and-a-half decades, the space physics community has developed a hard-earned and quite remarkable picture of the magnetosphere. This has been accomplished primarily by means of a continuing synthesis of satellite and ground-based observations, multipoint measurements, data analyses, and statistical results. The present picture, shown in figure 1, contains a host of plasma populations, energetic particle distributions, magnetic fields, electric fields, and electromagnetic waves that comprise the many distinct component regions of the magnetosphere—regions not dreamed of prior to the flight of the Explorer 1 satellite. In recent years, the quest for a global view has been further pursued through modeling and simulation. Both of these approaches, synthesis and modeling/simulation, have been quite successful in providing not only a summary of past observations and a valuable guide to future measurements but also tantalizing hints as to the global behavior of the magnetospheric system.

However, with the exception of auroral imagery, the global magnetosphere has remained invisible. There is no direct image of either the static or dynamic magnetosphere. Consequently, our quest for a global view remains unfulfilled. We are as limited as the proverbial blindmen examining an elephant. In magnetospheric physics, that is our present position—we have examined localized segments of the whole, yet have no accurate global perspective (Williams, 1990). The global pictures inferred from our syntheses and the results of our modeling/simulation efforts are helpful; however, without actual global observations, cartoons and simulations represent our global horizons. The lack of true global observations will always severely restrict our knowledge of the large-scale magnetosphere, and without an accurate global perspective, our progress toward understanding the magnetosphere and its dynamics will always be limited.

This then is the major over-arching goal of the MI program: to provide the first global observational picture of the magnetosphere, its major component parts, and its dynamics. Specifically, MI will combine simultaneous images of the major particle populations of the inner magnetosphere (Van Allen radiation belts, ring current, plasmasphere, inner plasmasheet) with auroral images to develop an initial picture of the magnetosphere, its interconnections, and its time variations. The new magnetospheric view to be generated from these global observations can be expected to be as surprising as the original discovery of the Earth's radiation belts.

Toward Fulfilling the Quest: This need for a global perspective is not unique to space physics, it is universal. It is required to place local observations and phenomena into an overall context, to understand how local processes combine to form the whole, and to provide comparisons with other globally observed phenomena. In magnetospheric physics we now are able to begin fulfilling this need. Recent instrumentation developments, as described later in this report, make it possible to obtain global images of major regions of the magnetosphere, and with time resolutions appropriate for the dynamics of the region being imaged.

The MI Science Definition Team (MI/SDT) proposes an MI satellite to provide the first systematic global images of the magnetosphere. Specifically the following major scientific objectives will be pursued within the context of the main MI goal described above:

- GLOBAL PICTURE: to understand the global shape and dynamics of the inner magnetosphere using simultaneously obtained images of the Earth's magnetosphere and its components (the ring current, the inner plasmasheet, the plasmasphere, the aurora, and the geocorona).

- GLOBAL RESPONSE: to learn how magnetospheric current systems, field configurations, and conductivities derived from images respond on a global scale to internal and external influences.

- GLOBAL MAPPING: to visualize and identify the connections of various magnetospheric components to each other, especially as these connections act to change the components during substorms and solar wind variations.

- GLOBAL FRAMEWORK: to relate global images of the magnetosphere to local observations in order to (a) learn how local processes combine to form the whole, (b) provide a global framework within which to place local observations, and (c) provide a "ground-truth" for the global observations.

Exploration and Discovery: The MI mission represents a mission of exploration and discovery that promises to be as dramatic as the first Explorers were with their forays into the radiation belts and beyond. Not only will the MI images provide the first large-scale visualization of the magnetosphere and its component parts, but the time sequencing of MI images will also provide the first visualization of magnetospheric dynamics on a large scale.

Extensive literature now exists on the need for global magnetospheric measurements, their expected science value, examples of early results, and global measurement techniques (Williams, 1990; Williams et al., 1992; Frank et al., 1982; Frank and Craven, 1988; Keath et al., 1989; McEntire and Mitchell, 1989; Hsieh and Curtis, 1989; Roelof et al., 1985, 1992, 1993; Roelof, 1987, 1989; Roelof and Williams, 1988; Williams et al., 1986; McComas et al., 1991, 1992; Moore et al., 1992; Funsten et al., 1992; Weller and Meier, 1974). Using this literature, we now demonstrate the value and power of macroscopic magnetospheric observations by presenting two specific previously reported simulations of imaging measurements expected to be obtained with presently available instruments. Figures 2 and 3 show, respectively, simulations of an active plasmasphere imaged in the He^+ (30.4 nm) line and the storm-time ring current imaged in hydrogen (H) and oxygen (O) ENA. These simulations are computed from models of the ion distributions derived from statistical compilations of 30 years of ground-based and in situ measurements. The models we have used are described in recent reviews of imaging (Meier, 1991; Williams et al., 1992). In order to present an overall perspective, we show both images from the same vantage point in a typical MI orbit—the premidnight sector at 5 R_E radius and 60° magnetic latitude. The Sun is on the upper left of the figures and the terminator is drawn on the Earth's surface. The color bars are logarithmic, covering a factor of 10^3, and are normalized to the maximum in the images. For He^+ (30.4 nm), the maximum intensity is 20 R. The ENA intensity is not specified in physical units because the intensities depend on the choice of species and the energy selected. However, since this ENA image is based on the actual ENA image obtained during a major geomagnetic storm (Roelof, 1987), we can say that the maximum intensity for either 25 to 35 keV H or 60 to 77 keV O would be $>10^4$ $(cm^2\ s\ sr)^{-1}$.

The simulated images include several commonly discussed physical features that are of major scientific interest because they are important manifestations of the global electrodynamics of the active magnetosphere. Although these features have been either synthesized, derived, or inferred from ground-based and/or in situ measurements, they have not yet been observed on a global basis. Clearly, actual images will, by inspection, resolve major unanswered questions concerning the global nature of these

regions, the plasmasphere and the ring current. For example, (1) large-scale plasmaspheric asymmetries will be seen, (2) the existence and global nature of plasmaspheric tails and/or ripples and/or detached plasma regions will be determined, (3) ring current injection boundaries will be observed, and (4) global ring current asymmetries will be measured.

Quantitative Results: As global magnetospheric observations have not yet been made, the MI mission is, as discussed above, one of exploration and discovery. However, the availability of global images and their time evolution allows, for the first time, the quantitative extraction of fundamental magnetospheric parameters on a global basis. For example, the simultaneous availability of time sequenced images of the plasmasphere and energetic ion populations provides the possibility of inferring the global electric and magnetic field configurations in the inner magnetosphere and their time evolution.

A further example of quantitative parameter extraction from magnetospheric global images is that of the global current distributions that are driven by the existing magnetospheric ion populations. To balance the pressure gradients of the ion distribution, currents must flow transverse to the magnetic field. These currents are related to the ion pressure tensor in the magnetic field and have been described by Parker (1957) in terms of ion pressures perpendicular and parallel to the field. Since the pressure tensor can be obtained from the ion distributions inferred from the MI images, the transverse current due to this distribution can be calculated. Assuming current conservation, the field aligned current can also be obtained.

Roelof (1989) has described a technique, along the lines described above, through which the global current system can be inferred from a global image of the magnetospheric energetic ion distribution. Applying this technique to the September 29, 1978, geomagnetic storm (for which he obtained the first rough image of the magnetospheric ring current (Roelof, 1987)), Roelof has obtained an estimate of the global current system established by the energetic ion distribution existing at the time. This inferred current system is shown in figures 4 and 5. Figure 4 presents two views of electrical current lines selected from the global system and that enter the ionosphere at 60° magnetic latitude. Figure 5 shows contours of field-aligned current density entering the ionosphere from the global current distribution. These contours are similar in polarity, strength, and shape to specific ionospheric currents, known as Region 2 currents (Iijima and Potemra, 1976, 1978), that have been statistically sampled by low-altitude, high-inclination satellites. Being the first attempt, the results of figures 4 and 5 are but the first rough approximation of what the actual global magnetospheric ring current may look like. Even so, these results carry great promise for a new and quantitative understanding of global magnetospheric behavior through the use of global observations.

Time Variations: The greatest obstacle in all our attempts to synthesize an accurate global picture of the magnetosphere is its time variability. Major regions of the magnetosphere can alter significantly their shape, composition, and interconnectivity over time scales far shorter than our capability to observe them by in situ measurements. The vast size of the magnetosphere will, in all probability, always preclude the establishment of a sufficiently dense network of in situ observations to accurately measure the global magnetosphere.

MI will provide spatially resolved images of the magnetosphere and its component parts, showing features such as those seen in figures 2 and 3, with time resolutions appropriate to the region and/or feature being observed. To demonstrate the global variations that might be expected during a geomagnetic storm, a technique developed by Roelof et al. (1993) is used whereby plasma densities and energetic particle fluxes generated by the Rice magnetospheric specification model (MSM), a derivative of the Rice convection model (RCM), are used as input for MI image simulations. The MSM uses actual magnetic storm data as input to generate the evolution of magnetospheric particle populations. The main difference between the MSM and the RCM is that the MSM, to save computing time, uses an empirical data-driven calculation to obtain the ionospheric electric field rather than the more rigorous self-consistent calculation of the RCM. However, the resulting magnetospheric particle populations obtained from the MSM are, when compared to RCM results, sufficiently accurate for the purpose of demonstrating MI capabilities for imaging the inner magnetosphere and its component parts.

These results have been reported earlier (Frank, Williams, and Roelof, 1993) and have recently been incorporated into a series of videos that dramatically show the time evolution of the MSM magnetosphere during a magnetic storm as imaged by available instruments (Roelof et al., 1994). Figure 6 shows a series of snapshots from the storm-time evolution of the ring current, a major subset of the radiation belts. ENA images of the Earth's inner magnetosphere are calculated using the MSM for the geomagnetic storm of April 21 to 22, 1988, as it would be imaged from 2.6 R_E at N60° in the dawn meridian. Three species, 30 keV H^+, 3 keV H^+, and 14 keV O^+, are shown for the three storm phases, prestorm, injection, and drift/convection in the recovery phase. Structural and global differences between the species shown are clearly seen in the injection and recovery phases as the particle populations are accelerated and driven by global electromagnetic forces. Note that not only will such ring current images be available for other energies and species, but they will be obtained simultaneously with images of the plasmasphere, the inner plasmasheet, and the aurora. Further, these images will be obtained throughout the storm on a continuous basis with a resolution of a few minutes. The resulting image set will provide the first opportunity to develop an accurate visualization of the dynamic evolution of these macroscopic magnetospheric regions.

Impact: Given the enormous influence of visual information on human insight and knowledge, the dissemination of the first images of the magnetosphere promises to change the prevailing views and interpretations of the plasma universe from those based on local observations to those based on global, integrated, and interrelated concepts. Natural plasmas will be viewed thereafter as whole systems with boundaries, gradients, and connections to surrounding systems. In this way, MI opens a new window into the plasma universe.

The impact of looking through this new window and obtaining a new global perspective will be felt in all space science disciplines in which plasma physics is important. For example, through the global images received, it is expected that the MI will provide a totally new perspective, both quantitatively and qualitatively, on the global and macroscale features of the magnetosphere and how it maps into the ionosphere/ thermosphere/mesosphere (ITM) regions. New imaging results that pertain to parameters such as global electrical conductivity, key elements of the global electric circuit, and global energy deposition into the upper atmosphere, will directly influence work in the ITM disciplines.

Similarly, the expected new magnetospheric perspectives and understanding obtained from the use of both global and local observations will be directly applicable to considerations of the formation and evolution of large-scale magnetic/plasma features in the solar corona. Solar physics should thus reap many of the benefits expected from the MI mission.

MI results will be applicable to astrophysical plasma systems that typically emit nonthermal radiation that is remotely observed (e.g., x rays, radio waves, and cosmic rays). The Earth's magnetosphere is one such nonthermally radiating system, and it has three highly desirable attributes for study. First, it is accessible to direct, local probing of its plasma, fields, and energetic particle content. Secondly, as with distant astrophysical systems, it can be remotely imaged. Thirdly, the Earth's magnetosphere consists of a rotating, magnetized object embedded in a high-speed stellar plasma outflow; a situation that gives rise to hot plasmas, energetic charged particles, ENA's, radio waves, x rays, and FUV emissions. It remains for MI to provide the initial global perspective and, in conjunction with local observations, to present the beginning of a quantitative understanding of the overall system.

Finally, the MI results will be applicable directly to other planetary magnetospheres. It is important to realize the synergism of comparing the Earth to other solar system objects. Earth-based images of the sodium nebulae of Mercury's and Jupiter's magnetospheres have already been obtained. Magnetospheric imagery of Saturn will be provided on the Cassini mission. MI observations will provide a key link in the development of systematic comparative planetology, especially in the formation and dynamics of planetary magnetospheres and their interactions with planetary atmospheres, rings, and satellites.

References

Frank, L.A., and Craven, J.D. (1988): "Imaging Results from Dynamics Explorer 1." Rev. Geophys., vol. 26, p. 249.

Frank, L.A., Craven, J.D., Burch, J.L., and Winningham, J.D. (1982): "Polar Views of the Earth's Aurora with Dynamics Explorer." Geophys. Res. Lett., vol. 9, p. 10001.

Frank, L.A., Williams, D.J., and Roelof, E.C. (1993): "Imagers for the Magnetosphere, Aurora and Plasmasphere (IMAP)." Instrumentation for Magnetospheric Imagery II, Proc. SPIE, S. Chakrabarti (ed.), p. 2008.

Funsten, H.O., McComas, D.J., and Barraclough, B.L. (1992): "Application of Thin Foils in Low Energy Neutral Atom Detection." Instrumentation for Magnetospheric Imagery, SPIE Proc., vol. 1744, p. 62.

Hsieh, K.-C., and Curtis, C.C. (1989): "Remote Sensing of Planetary Magnetospheres: Mass and Energy Analysis of Energetic Neutral Atoms." Solar System Plasma Physics, J.H. Waite, Jr., J.L. Burch, and R. L. Moore (eds.), Geophys. Monogr. Ser., No. 54, p. 159, AGU. Washington, DC.

Iijima, T., and Potemra, T.A. (1976): "Field Aligned Currents in the Dayside Cusp Observed by Triad." J. Geophys. Res., vol. 81, p. 5971.

Iijima, T., and Potemra, T.A. (1978): "Large-Scale Characteristics of Field-Aligned Currents Associated With Substorms." J. Geophys. Res., vol. 83, p. 599.

Keath, E.P., Andrews, G.B., Mauk, B.H., Mitchell, D.G., and Williams, D.J. (1989): "Instrumentation for Energetic Neutral Atom Imaging of Magnetospheres." Solar System Plasma Physics, Geophys. Monogr. Ser., vo. 54, p. 165, AGU, Washington, DC.

McComas, D.J., Barraclough, B.L., Elphic, R.C., Funsten, H.O. III, and Thomsen, M.F. (1991): "Magnetospheric Imaging With Low Energy Neutral Atoms." Proceedings of the National Academy of Sciences, USA, vol. 88, p. 9589.

McComas, D.J., Funsten, H.O., Gosling, J.T., Moore, K.R., and Thomsen, M.F. (1992): "Low Energy Neutral Atom Imaging." Instrumentation for Magnetospheric Imagery, SPIE Proc., vol. 1744, p. 40.

McEntire, R.W., and Mitchell, D.G. (1989): "Instrumentation for Global Magnetospheric Imaging Via Energetic Neutral Atoms." Solar System Plasma Physics, J.H. Waite, Jr., J.L. Burch, and R.L. Moore (eds.), Geophys. Monogr. Ser., No. 54, p. 69, AGU, Washington, DC.

Meier, R.R. (1991): "Ultraviolet Spectroscopy and Remote Sensing of the Upper Atmosphere." Space Sci. Rev., vol. 59, p. 1.

Moore, K.R., McComas, D.J., Funsten, H.O., and Thomsen, M.F. (1992): "Low Energy Neutral Atoms in the Earth's Magnetosphere: Modeling, Instrumentation for Magnetospheric Imagery, SPIE Proc., vol. 1744, p. 51.

Parker, E.N.(1957): "Newtonian Development of the Dynamical Properties of Ionized Gasses at Low Densities." Phys. Rev., vol. 107, p. 924.

Roelof, E.C.(1987): "Energetic Neutral Atom Image of a Storm-Time Ring Current." Geophys. Res. Lett., vo. 14, p. 652.

Roelof, E.C.(1989): "Remote Sensing of the Ring Current Using Energetic Neutral Atoms." Adv. Space Res., vol. 9, No. 12, p. 195.

Roelof, E.C., and Williams, D.J. (1988): "The Terrestrial Ring Current: From In Situ Measurements to Global Images Using Energetic Neutral Atoms." Johns Hopkins APL Tech. Dig., vol. 9, p. 144.

Roelof, E.C., Mitchell, D.G., and Williams, D.J. (1985): " Energetic Neutral Atoms (E ~ 50 keV) From the Ring Current: IMP 7/8 and ISEE 1." J. Geophys. Res., vol. 90, p. 10991.

Roelof, E.C., Mauk, B.H., and Meier, R.R. (1992): "Instrument Requirements for Imaging the Magnetosphere in Extreme-Ultraviolet and Energetic Neutral Atoms Derived From Computer-Simulated Images." Instrumentation for Magnetospheric Imagery, Proc. SPIE, S. Chakrabarti (ed.), vol. 1744, pp. 19–30.

Roelof, E.C., Mauk, B.H., Meier, R.R., Moore, K.R., and Wolf, R.A. (1993): "Simulations of EUV and ENA Magnetospheric Images Based on the Rice Convection Model." Instrumentation for Magnetospheric Imagery II, Proc. SPIE, S. Chakrabarti (ed.), vol. 2008, pp. 202–213.

Roelof, E.C., Mauk, B.H., Chase, C.J., Mitchell, D.G., Williams, D.J., Sussman, D.W., Hobson, L.J., Wolf, R.A., and Spiro, R.W. (1994): "Energetic Neutral Atom Images of a Geomagnetic Storm: A Computer-Simulated Visualization." JHU/APL Video, January.

Weller, C.S., and Meier, R.R. (1974): "First Satellite Observations of the He^+ 304-Å Radiation and Its Interpretation." J. Geophys. Res., vol. 79, p. 1572.

Williams, D.J. (1990): "Why We Need Global Observations." Magnetospheric Physics, B. Hultqvist and C. G. Falthammer (eds.), Plenum, New York, p. 83, Plenum, New York.

Williams, D.J., Frank, L.A., Broadfoot, A.L., Imhoff, W.L., Mende, S.B., Hunten, D.M., Roble, R.G., and Siscoe, G.L. (1986): "Images of Magnetosphere and Atmosphere: Global Effects (IMAGE)." Proposal to NASA for the IMAGE Explorer Mission Concept, July.

Williams, D.J., Roelof, E.C., and Mitchell, D.G. (1992): "Global Magnetospheric Imaging." Rev. Geophys., vol. 30, No. 3, p. 183.

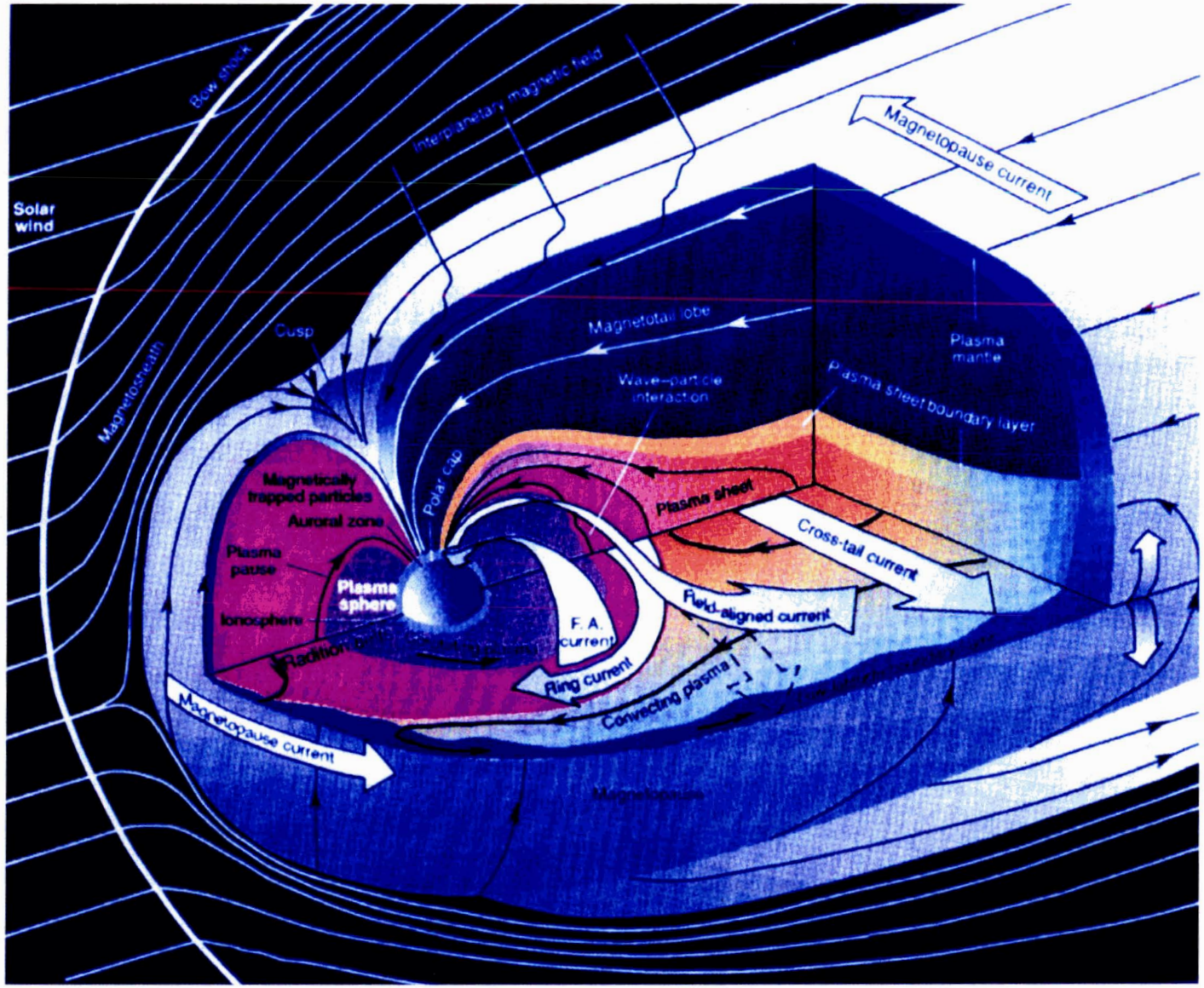

A popular schematic, generaly accepted as portraying the Earth's magnetosphere and its major components.

Figure 1. Schematic of magnetosphere (artist's concept).

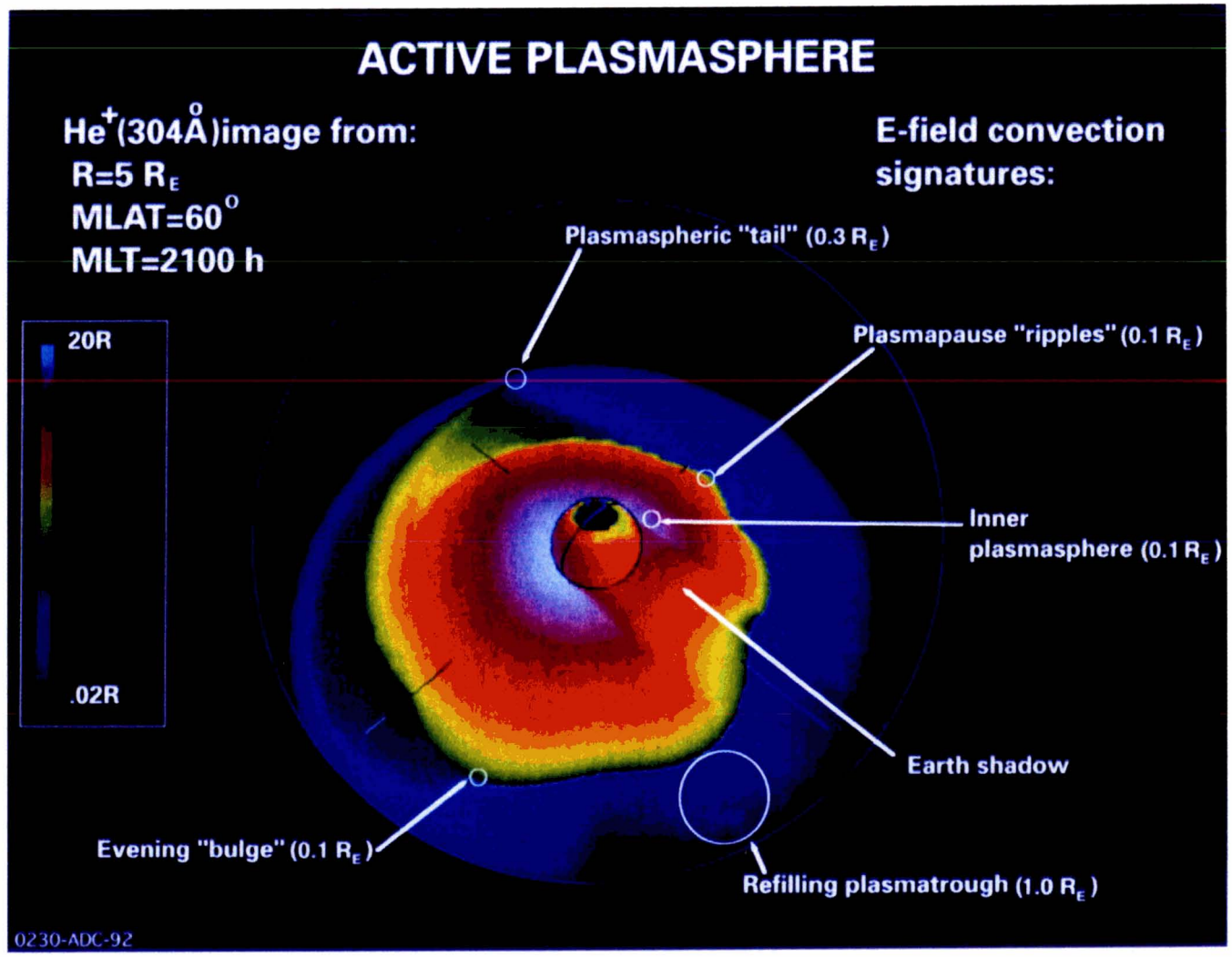

Simulation of an "active" plasmasphere image based on presently available instrument capabilities. The vantage point is in the premidnight sector at a radial distance of 5 R_E and 60° magnetic latitude. The Sun's direction is to the upper left, and the terminator is shown on the Earth's surface. The image is obtained from He^+ (30.4 nm) resonantly scattered radiation. The logarithmic color bar spans a factor of 10^3 in intensity and is calibrated directly in Rayleighs (R). Structures that provide signatures of global electric-field convection patterns are easily identified.

Figure 2. Active plasmasphere.

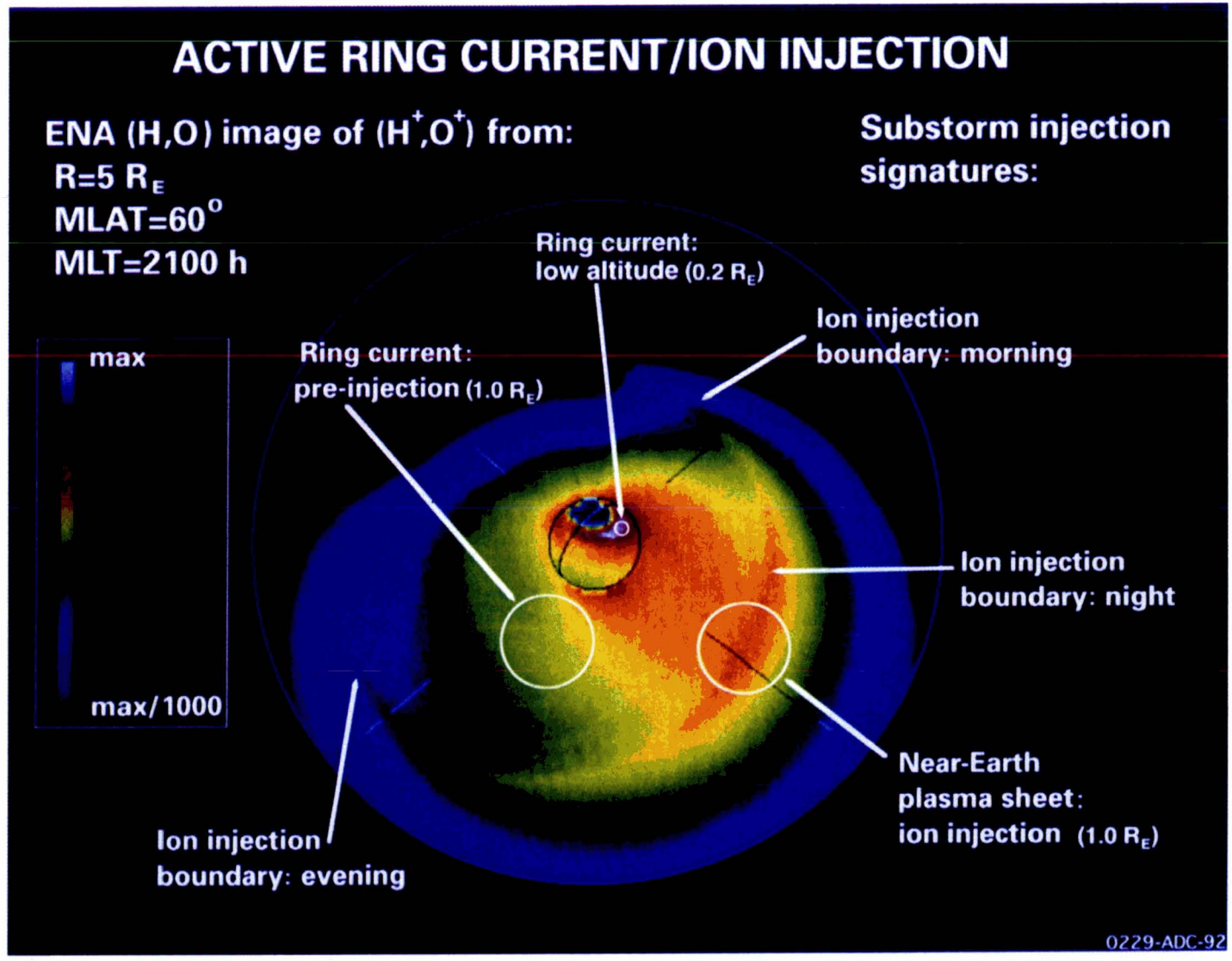

Simulated ENA image of an active ring current/ion injection. The logarithmic color bar spans a range of 10^3, normalized to the maximum ENA flux in the image. The vantage point is the same as in figure 1. Superimposed upon a recovery-phase ring current is a new energetic ion injection from the near-Earth plasma sheet.

Figure 3. Active ring current/ion injection

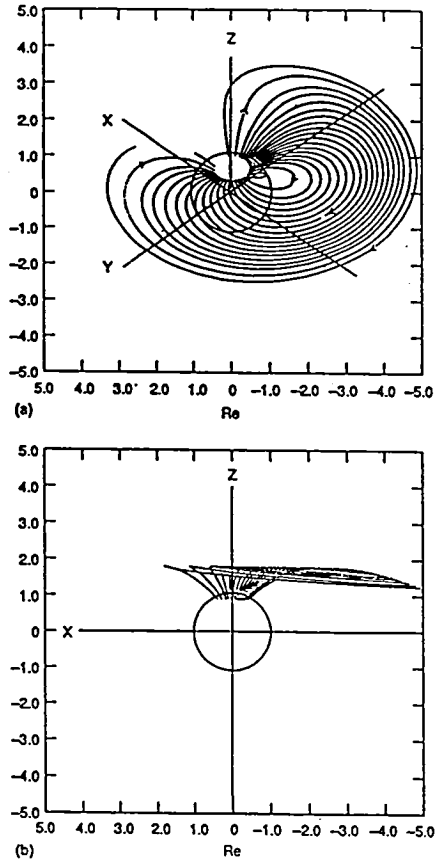

Two views of selected electric current lines resulting from the global ion distribution inferred for the magnetic storm of September 29, 1978. The current lines shown are those that intersect the ionosphere at 60° magnetic latitude. Spacing represents current density (from Roelof, 1989).

Figure 4. Two views of global current system that enters the ionosphere at 60° N.

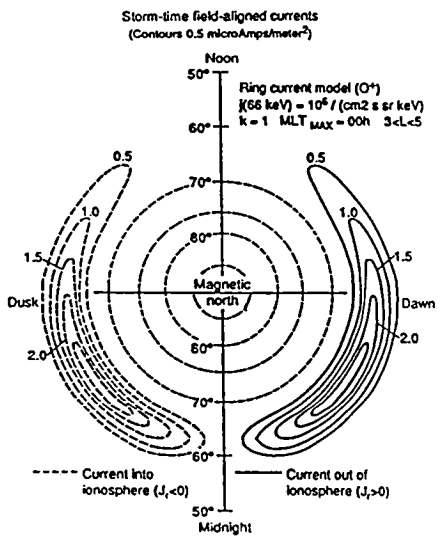

Contours of field-aligned current density entering the ionosphere from the current distribution responsible for the electric current lines shown in figure 5. The latitude, direction, and intensity resemble those of region two currents measured during disturbed times (from Roelof, 1989).

Figure 5. Contours of storm-time field-aligned current entering the ionosphere.

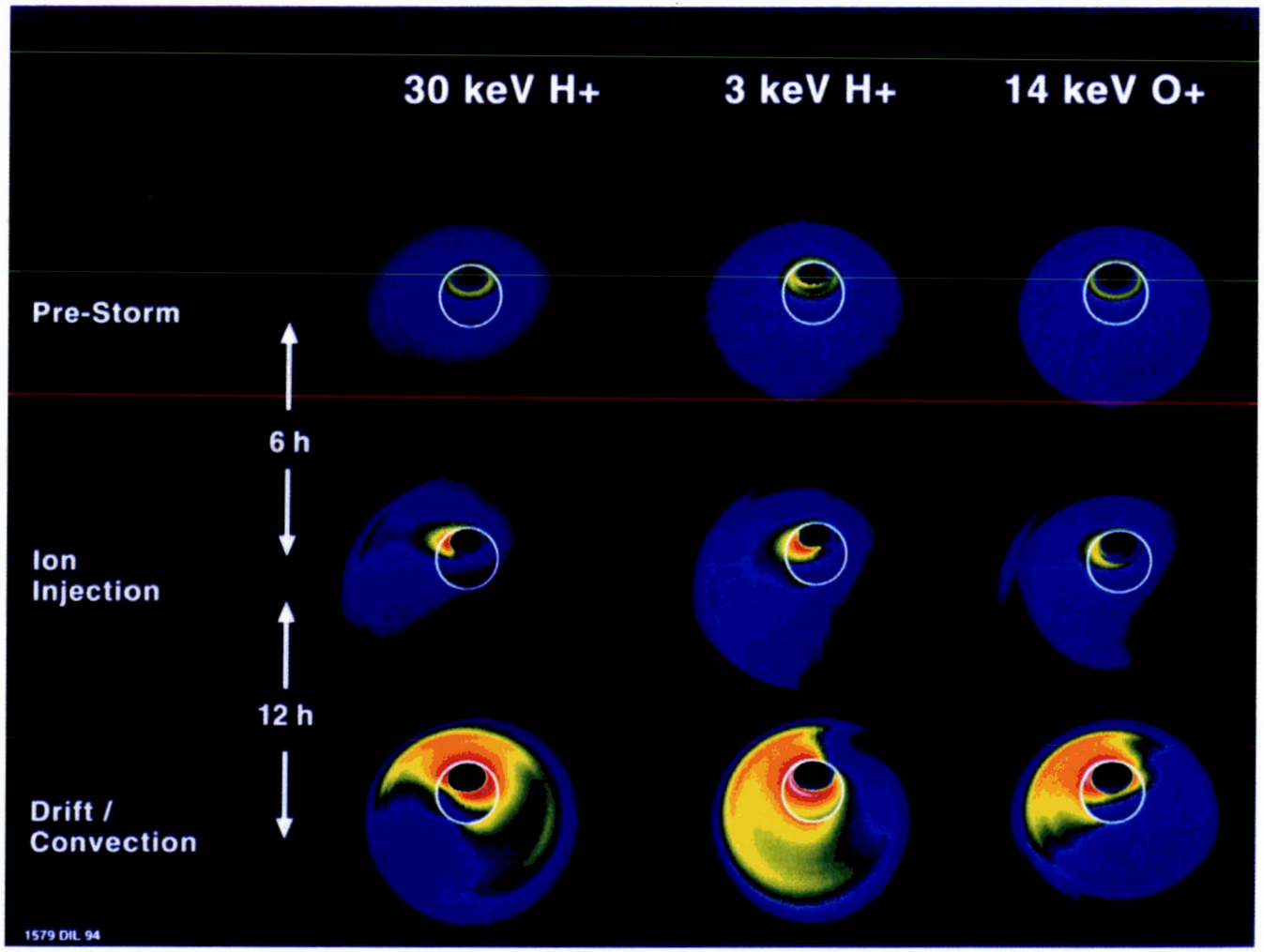

Series of ENA snapshots from JHU/APL computer-simulation video. ENA images of the Earth's magnetosphere are calculated using the Rice University Magnetospheric Specification Model for the geomagnetic storm of April 21 to 22, 1988, as it would be imaged from 2.6 R_E and N60° in the dawn meridian (noon is to the right). Three species and three storm phases are shown. Global differences can be seen in the evolution of the three populations shown. In actuality, a much more continuous evolution is observed, providing a detailed measure of the changing configurations. Images at other energies and species as well as simultaneous images of the plasmasphere and aurora will be available from eventual imaging missions.

Figure 6. Storm-time evolution of 30- and 3-KeV H^+ and 14- keV O^+

METHODS OF IMAGE INTERPRETATION APPLICABLE TO MI

Image Processing, Interpretation, and Inversion

1. The New Window—Plasma Imaging

The MI mission will provide data in the form of two-dimensional (2–D) images of the inner magnetosphere: the ring current, the plasmasphere, the inner plasma sheet, and the auroral ionosphere. These regions are astrophysical-class plasmas that exhibit the same basic plasma mechanisms that are operative in plasmas throughout the universe. Since no global scale images of these regions exist in even moderate resolution, the MI mission is first and foremost an exploratory mission that will resolve long-standing controversies in magnetospheric physics by providing new views of the terrestrial plasma environment. Hitherto unobservable causal relationships among plasma processes will be revealed in different regions of the magnetosphere. This macroscale exploration of astrophysical class plasmas will be similar to the great leap forward in the understanding of solar system planets and their moons made possible by deep space probe images.

For each of the imaging instruments on MI, the data stream will contain information on specific pixel sizes, pixel intensities, photon or particle energy bandwidth, and integration period. Preprocessing of this information will involve techniques such as validating data quality, removing systematic noise, accounting for missing data, and mapping onto an image format for ready visual display. The images can then be processed to provide high-quality visual display and videos suitable for recognition of magnetospheric phenomena. It will be possible to see directly in the images such features as the hot ring current regime, the plasmapause, regions of cold detached plasma, the inner plasma sheet and substorm particle acceleration phenomena, the dynamic auroral oval, and, most importantly, the simultaneous response of the different magnetospheric regions to external forcings. These images will be released promptly to the scientific community and the public to provide awareness of "space weather" and its impact on the global environment. It is at this stage that many new discoveries are expected since the images will reveal a perspective of astrophysical plasmas never before seen.

At least two levels of interpretation are possible with the processed images. The first level interpretation includes pattern recognition in the assignment of "meaning" to the images. Since some features in the images will not require a high level of interpretation, the observations could be combined with ancillary information such as rudimentary models to form a phenomenological approach for recognizing relationships among magnetospheric regions. This will form the basis for qualitative understanding of morphological features. It may even be possible to develop new indices of geomagnetic activity more relevant for ordering in situ data. A higher level of pattern recognition could be implemented through use of logical systems such as neural networks.

At the second level of interpretation, actual image inversion will be implemented to extract quantitative information on the inner magnetosphere. This can be accomplished by using forward models of the individual magnetospheric regions combined with inversion methods to retrieve parameters of the models from the data. For example, plasma simulation models could be used directly in the inversion process, although they are currently too computationally expensive for this purpose. More practical is the use of parameterized models, whose parameters can be related to variables in the physical models. This inversion methodology will permit the retrieval of three-dimensional (3–D) information about magnetospheric systems from 2–D images. Additionally, many inversion techniques incorporate formal procedures for estimating the uncertainties in the parameters due to uncertainties in the observations and the models. The parameter uncertainties can, in turn, be mapped into uncertainties in physical quantities, such as the plasma concentration, using propagation of errors.

Data products from MI will not only include the images themselves, but also time sequences of morphological parameters deduced from the first level of interpretation, and retrieved parameters of models. The constrained models can be used to provide higher level data products such as images and

videos of plasma distribution and currents, electric field convection, particle energization, and ionospheric conductivities.

2. Image Processing

As indicated above, preprocessing involves the production of first-level images from the MI data stream. The actual image processing is concerned primarily with image enhancement to improve pattern recognition, either by humans or automated systems. Usual image enhancement techniques include averaging, filtering, masking, contrast stretching, and grey-scale transforming. The use of false color can bring out weak or unrecognized features in images, as well. The processing method is chosen to suit the end product. For automated pattern recognition, it is best to enhance the morphological features desired. For human interaction, certain false color displays provide instant recognition of familiar patterns. For scientific analysis, filter application or masking may be desirable to suppress background or foreground emissions.

At this stage, it may be advantageous to transform from the initial pixel coordinate system observed from MI to alternative coordinate systems (e.g., B, L, MLT) for systematic comparison and better ordering of images from different parts of the inner magnetosphere. Interpretation will be enhanced by the use of superimposed coordinate grids. Inclusion of ancillary data, such as solar wind, IMF, ground-based rheometer data, etc., will take place at this level.

3. New Discoveries

A new level of exploratory science will be available from the processed images. No global views of the ring current, the plasmasphere, or the inner plasma sheet have been seen before. An extensive number of observational "firsts" will be forthcoming.

By visual comparison of image sequences, the time variation of the spatial extent and the intensity of the ring current, the plasmasphere, and the inner plasma sheet will be possible on substorm to storm-time scales. The temporal correlation between ring current and auroral dynamics will similarly be evident. For the first time, a true local time dependence will be established for differentiating local time asymmetries, such as the evening sector activity in the plasmasphere (formerly referred to as the "bulge" because the density variations could not be resolved by in situ spacecraft measurements). During storms/substorms, "detached" regions of plasma will be clearly evident. The injection history leading to the formation of the storm-time ring current will be seen for the first time, as will the complex evolution of multiple substorms and injection boundaries. The correlation of such spatial structure with the corresponding auroral structure will give unique insights into the fine structure of the magnetospheric substorm/storm.

Images and videos of these new discoveries can be made available to support programs in space weather monitoring. They can also be used to provide public awareness of space weather and its impact on society. They are a natural resource for introducing space physics into the kindergarten to 12th grade classroom.

4. Pattern Recognition and Interpretation

Image enhancement for morphological interpretation often does not progress beyond the preprocessing or initial processing stages. On the other hand, much quantitative information will be present in the simultaneous images of the ring current, the plasmasphere, the inner plasma sheet, and the aurora that will be difficult to detect by eye. Sophisticated techniques, such as neural networks, have been developed not only to "learn" how systems behave in general and to recognize routine scenes, but also to detect unusual activity patterns which may not be evident to the human observer.

For the magnetosphere systems, a neural network could not only identify and predict coupling among features in the individual images, but also could incorporate such ancillary data as the IMF direction or the solar wind flux and learn to recognize responses within the images to those external inputs. When

certain patterns are recognized and characterized by an automated system, new insights into the behavior of the various systems will result. The phenomenology will force the development of new models that properly incorporate the physics needed to explain the images.

5. Image Inversion

Because the different regions of the inner magnetosphere are not sampled simultaneously from many directions by MI, full tomographic inversions are not feasible. The data therefore consist of a series of 2–D images of 3–D phenomena. In order to optimize the 3–D information return from the data, image inversion is required. The inversion process begins with observational data and a forward model from which optimal values of model parameters, as well as their uncertainties, can be retrieved. The models should contain sufficient parameters to describe the physical processes. Unfortunately, the first principles physical models are computationally intense and not suitable for the rapid calculations needed in an inversion model. Alternatively, ad hoc models can also be used. Initial work has utilized parameterized models that are based on statistical plasma distributions derived empirically using in situ data. The model parameters are used to rescale various aspects of the distributions; for example the radial distances to distribution boundaries. Retrieved values for the parameters can then be used to constrain physical models. The advantage of simple parameterized models is that the inversion algorithms are sufficiently rapid and robust that they can be automated for routine production of data products. In any inversion process, it is essential to incorporate estimates of the uncertainties of the retrieved parameters due to uncertainties in the data and in the models. Formal methods exist for doing so (Tarantola, 1987; Menke, 1989).

In each of the three principal regions sampled by MI, the understanding of the microscopic processes leading to the production of radiation or ENA's has advanced sufficiently that algorithms exist that can synthesize images (Williams, 1990; Roelof et al., 1993). The algorithms employ parameterized representations of the concentrations of species responsible for the production of the photons or particles to be imaged. Examples of inversion approaches are described in the following subsections.

5.1. Inversion of ENA Images. Significant progress has been made in developing an inversion algorithm for ENA images (Roelof et al., 1993). Tests have been made using the Rice University magnetospheric specification model (MSM) to provide synthetic images ("data"). The data image is generated with the angular resolution that an actual ENA camera could easily achieve. Ion intensities are specified as functions of L for various magnetic local times. Roelof et al.(1993) described a 10 parameter model of the ion intensity which has sufficient flexibility to represent the principal features of the MSM. In this example, the goal of the inversion process is to use the "observed image" to provide the best estimate of each of the 10 parameters. The algorithm chosen for this example was Powell's method as improved by Acton (Press et al., 1989). The retrievals have been shown to be robust against the effects of noise and background (Roelof et al., 1992).

It was concluded that these initial attempts at ENA image inversion show great promise for automated retrieval of ring current parameters from even a single image. Actually, a complete suite of images (each pixel measured in a spectrum of ENA energies) would contain much more physical information than any single image of any single species at any single energy. The method of "sequential optimization" (e.g., Kalman filtering; Press et al., 1989) can be used to relate the information among successive images.

5.2. Plasmaspheric Image Inversion. Although the algorithms for inverting He^+ 30.4 nm images are still in the development phase, the approach is similar to that of ENA image inversion. Simple parameterized models of the plasmasphere have already been developed (Meier and Weller, 1972; Roelof et al., 1992). The parameters consist of the ion concentration at 1,000 km, the plasmapause L-value, its local time variation, the ion concentration fall-off beyond the plasmapause, the concentration variation with latitude and other parameters describing such features as the dusk "bulge" activity region, and the daytime "tail."

The absolute value of the intensity is of less consequence than the morphology, which is the most important quantity for deduction of global information about the plasmasphere. The problem, then, is to

extract the helium ion distribution from EUV images. The absolute magnitude of the helium ion abundance can, nonetheless, be determined to within a factor of 2 or so using proxies for the incident solar irradiance.

Application of the inversion algorithm follows the ENA process described in section 5.1. Data are used to extract the optimum set of parameters, and their uncertainties are derived from the uncertainties in the observations, the forward model, or from any a priori information needed to constrain underdetermined parameters. Meier and Picone (1994) and Picone et al. (1994) have shown that the retrieval methodology is robust for a wide variety of applications. Garrido et al. (1993) have developed a matrix method for inverting high-latitude photometric observations of He^+ 30.4 nm radiation made from a rocket.

As with the ENA image inversion, the retrieved parameters can be used in turn to constrain first principles models of the plasmasphere. Alternatively, empirical models of the plasmasphere are now under development. These will contain parameters that could easily be incorporated into inversion algorithms.

5.3. Auroral Imaging. Advanced algorithms have already been developed that relate FUV emission line and band spectra to the characteristic energy and energy flux of precipitating electrons in auroras (Strickland et al., 1983; Germany et al., 1994; Meier and Strickland, 1991). Ratios of individual vibrational bands of the Lyman-Birge-Hopfield series of N_2 are sensitive to the penetration depth of auroral electrons and consequently to their characteristic energy. The energy flux is proportional to the column emission rate of the bands. Consequently, monochromatic or narrow-band images of N_2 bands can provide global maps of precipitating electron characteristics. The algorithms are most sensitive to precipitating electrons with characteristic energies of 0.5 keV up to at least 20 keV.

Once the character of the electron precipitation is known, ratios of atomic oxygen to N_2 emissions constrain the O/N_2 concentration ratios, thereby providing sufficient information to compute height-integrated ionospheric conductivities (Germany et al., 1994; Rees et al., 1988). For the relevant characteristic energies (>0.5 keV), the conductivities apply to the ionospheric E-region.

Precipitating proton fluxes can be inferred from hydrogen Lyman-α emission at 121.6 nm. Without a separate instrument with the capability of suppressing the foreground geocoronal emission, it is necessary to use the auroral imager to discriminate proton-generated emissions by their contrast against the geocoronal Lyman-α emission (Chubb and Hicks, 1970). No multiple scattering of proton-generated Lyman-α occurs because Doppler shifts move the radiation outside the core of the ambient hydrogen absorption line. Recent papers by Basu et al. (1993) and Strickland et al. (1993) report emission yields for Lyman-α, and for O and N_2 emissions as functions of characteristic energy of precipitating protons. For pure proton auroras, algorithms similar to those of Strickland et al. (1983) can be constructed to deduce the characteristic energy (from LBH bands) and the energy flux (from the Lyman-α emission rate). However, the proton aurora will often occur in the presence of the usually brighter electron aurora. In this case, the proton characteristic energy may not be determined, but the total proton energy flux is still provided by the Lyman-α intensities.

5.4. Inversion of Image Sequences. Much of the early work on image inversion has concentrated on the extraction of physical parameters from a single image. This is the most challenging problem mathematically, and it can be attacked successfully whenever it can be assumed that the imaged particle distribution can be ordered in a phase space coordinate system in which one or more coordinates are ignorable (for example, by making use of conservation of magnetic moment and energy to project pitch angle distributions along field lines). This reduces the dimensionality of the inversion problem.

In an actual mission, however, the majority of the images around the orbit will be obtained while magnetospheric plasmas are evolving slowly (on the time scale of an orbital period). This is particularly true of the global plasmasphere and plasmatrough, as well as the ring current and near-Earth plasma sheet outside of substorm activity. (Single images of substorm injection events are nonetheless extremely useful, because the entire image does not have to be mathematically inverted in order to deduce the time and location of the particle acceleration region—the most important information in the image). A sequence of

N images taken along the orbit during a period when the global magnetosphere is quasi-stationary will constitute an N-fold set of constraints on the inversion procedure (although their functional independence will depend on the range of viewpoints encompassed). The mathematical problem is more one of "partial tomography," in which the full armory of tools for complete (ideal) tomography (in which all possible aspects are viewed) still cannot be applied, but modified tools (supplemented by physics-based approximations) can be applied. A trivial example is parameter extraction by forward modeling, in which the weighted differences between all N images and their parameterized simulations would be minimized simultaneously.

5.5. Advanced Algorithms and Modeling. At first, the algorithms cited above will be applied independently to ENA, EUV, and FUV images from MI. But the retrieved parameters may not be self-consistent because although the different regions of the inner magnetosphere are coupled, their forward models and retrieval algorithms are not. For example, the parameterized models may contain overlapping boundaries, which should be self-consistent with physical interactions that occur there (e.g., wave/particle instabilities where the ring current and plasmasphere overlap). Thus, advanced algorithms may be needed that combine the data products from the individual retrievals and their uncertainties. If the uncertainties of similar parameters are not consistent, it will be necessary to combine the separate data sets and algorithms or to develop new models that take advantage of the combined information. The approach to be followed depends critically on the statistical significance of each pixel in an image. For example, a parameter retrieved from a plasmasphere image with high statistical accuracy may be used as a priori information to constrain other parameters to be retrieved from a ring current image.

From a more fundamental perspective, the plasma distributions derived via the inversions obtained from the multiple imaging techniques must be self-consistent in terms of the global electrodynamics problem of the Earth's magnetosphere. For example, magnetic field aligned electric currents derived from the hot-ring current population distributions must be self consistent with the global electric fields inferred from the distributions and evolutions of cold plasmaspheric populations, since the electric fields participate in the charge separations that give rise to the currents. Similarly, the inversions must reflect the anticipated auroral region response to the derived electric currents. Ultimately, global electromagnetic models must be brought into the process of establishing the self consistency of the inversions and utilized to make corrections to the inversion processes.

Obviously, new discoveries in the processed images will drive improvements in the parameterized models currently in use (which are based on statistical synoptic distributions derived from in situ observations). These improvements will become available as the physics in "first principle" models are updated by the modeling community to accommodate the new discoveries. The final product of the MI mission will be validated models of the dynamics of each plasma regime, as well as the coupling of these regions throughout the inner magnetosphere.

References

Basu, B., Jasperse, J.R., Strickland, D.J., and Daniel, R.E. (1993): "Transport-Theoretic Model for the Electron-Proton-Hydrogen Atom Aurora, 1. Theory." J. Geophys. Res., vol. 98, p. 21517.

Chubb, T.A., and Hicks, G.T. (1970): "Observations of the Aurora in the Far Ultraviolet From OGO 4." J. Geophys. Res., vol. 75, p. 1290.

Gallagher, D.L., Craven, P.D., and Comfort, R.H. (1988): "An Empirical Model of the Earth's Plasmasphere." Adv. Space Res., vol. 8, p. 15.

Garrido, D.E., Smith, R.W., Marsh, C.A., Christensen, A.B., and Chakrabarti, S. (1993): "Inversion of Photometric He^+ (30.4-nm) Intensities to Obtain He^+ Distributions." SPIE, vol. 2008, p. 121.

Germany, G.A., Torr, D.G., Richards, P.G., Torr, M.R., and John, S. (1994): "Determination of Ionospheric Conductivities From FUV Auroral Emissions." J. Geophys. Res., vol. 99, p. 23297.

Germany, G.A., Torr, M.R., Torr, D.G., and Richards, P.G. (1994): "Use of FUV Auroral Emissions as Diagnostic Indicators." J. Geophys. Res., vol. 95, p. 7725.

Meier, R.R., and Weller, C.S. (1972): "EUV Resonance Radiation From Helium Atoms and Ions in the Geocorona." J. Geophys. Res., vol. 77, p. 1190.

Meier R.R., and Strickland, D.J. (1991): "Auroral Emission Processes and Remote Sensing." Aurora, C. Ming, L. Frank, and M. Rycroft (eds.), Cambridge University Press.

Meier, R.R., and Picone, J.M. (1994): "Retrieval of Absolute Thermospheric Concentrations From the Far UV Dayglow: An Application of Discrete Inverse Theory." J. Geophys. Res., vol. 99, p. 6307.

Menke, W. (1989): "Geophysical Data Analysis: Discrete Inverse Theory." International Geophysics Series, No. 45, Academic Press, London.

Picone, J.M., Dymond, K.F., Meier, R.R., McCoy, R.P., and Kelley, O. (1993): "Retrieval of Daytime Ionospheric O^+ Distributions From OII 834 A Limb Intensities." Eos, vol. 74, p. 460.

Press, W.H., Flannery, B.P., Teukolsky, S.A., and Vetterling, W.T. (1989): "Numerical Recipes." Cambridge University Press, Cambridge.

Rees, M.H., Lummerzheim, D., Roble, R.G., Winningham, J.D., Craven, J.D., and Frank, L.A. (1988): "Auroral Energy Deposition Rate, Characteristic Electron Energy, and Ionospheric Parameters Derived From Dynamics Explorer 1 Images." J. Geophys. Res., vol. 93, p. 12841.

Roelof, E.C., Mauk, B.H., and Meier, R.R. (1992): "Instrument Requirements for Imaging the Magnetosphere in Extreme-Ultraviolet and Energetic Neutral Atoms Derived From Computer-Simulated Images." Proc. SPIE, Instrumentation for Magnetospheric Imagery, S. Chakrabarti (ed.), vol. 1744, p. 19.

Strickland, D.J., Book, D.L., Coffey, T.P., and Fedder, J.A. (1976): "Transport Equation Techniques for the Deposition of Auroral Electrons." J. Geophys. Res., vol. 812, p. 2755.

Strickland, D.J., Daniel, R.E., Basu, B., and Jasperse, J.R. (1993): "Transport-Theoretic Model for the Electron-Proton-Hydrogen Atom Aurora, 2. Model results." J. Geophys. Res., vol. 98, p. 21533.

Tarantola, A. (1987): "Inverse Problem Theory." Elsevier, Amsterdam.

Williams, D.J., Roelof, E.C., and Mitchell, D.G. (1992): "Global Magnetospheric Imaging." Rev. Geophys., vol. 30, p. 183.

BIBLIOGRAPHY ON MI

General Reviews and Special Issues

Frank, L.A., and Craven, J.D.: "Imaging Results from Dynamics Explorer 1." Rev. Geophys., vol. 26, 1988, p. 249.

Frank, L.A., Craven, J.D., Ackerson, K.L., English, M.R., Esther, R.H., and Carovillano, R.I.: "Global Auroral Imaging Instrumentation for the Dynamics Explorer Mission." Space Sci. Instrum., vol. 5, 1981, p. 369.

Frank, L.A., Williams, D.J., and Roelof, E.C.: "Imagers for the Magnetosphere, Aurora, and Plasmasphere (IMAP)." Proceedings of SPIE, Instrumentation for Magnetospheric Imagery II, S. Chakrabarti (ed.), vol. 2008, 1993, pp. 11–34.

Frank, L.A., Sigwarth, J.B., Williams, D.J., Roelof, E.C., Mitchell, D.G., Gold, R.E., Keath, E.P., Mauk, B.H., Meng, C.-I., Carpenter, D.L., Hultqvist, B.K., Lundin, R.N., Siscoe, G.L., Wolf, R.A., Gorney, D.J., Schulz, M., McComas, D.J., Funsten, H.O., Moore, K.R., Smith, B.W., Craven, J.D., Chiu, Y.T., Meier, R.R., and Seely, J.F.: "Imagers for the Magnetosphere, Aurora, and Plasmasphere." Optical Engr., vol. 33, 1994, p. 391.

Funsten, H.O., McComas, D.J., and Barraclough, B.L.: "Application of Thin Foils in Low Energy Neutral Atom Detection, Instrumentation for Magnetospheric Imagery." Proceedings of SPIE, Instrumentation for Magnetospheric Imagery II, S. Chakrabarti (ed.), vol. 1744, 1992, p. 62. Also submitted to Optical Science.

Gallagher, D.L.: "The Inner Magnetosphere Imager Mission." Solar System Plasmas in Space and Time, Geophys. Monogr. Ser., vol. 84, AGU, Washington, DC, 1994.

Hsieh, K.C., and Curtis, C.: "Remote Sensing of Planetary Magnetospheres: Mass and Energy Analysis of Energetic Neutral Atoms." Solar System Plasma Physics, Geophys. Monogr. Ser., vol. 54, J.H. Waite et al. (eds.), p. 159, AGU, Washington, DC, 1989.

Keath, E.P., Andrews, G.B., Cheng, A.F., Krimigis, S.M., Mauk, B.H., Mitchell, D.G., and Williams, D.J.: "Instrumentation for Energetic Neutral Atom Imaging of Magnetospheres." Solar System Plasma Physics, Geophys. Monogr. Ser., vol. 54, J. Burch and J. Waite (eds.), p. 165, AGU, Washington, DC, 1989.

McComas, D.J., Barraclough, B.L., Elphic, R.C., Funsten, H.O. III, and Thomsen, M.F.: "Magnetospheric Imaging With Low-Energy Neutral Atoms." Proc. Natl. Acad. Sci. USA, vol. 88, 1991, p. 9598.

McComas, D.J., Funsten, H.O., Gosling, J.T., Moore, K.R., and Thomsen, M.F.: "Low Energy Neutral Atom Imaging, Instrumentation for Magnetospheric Imagery." Instrumentation for Magnetospheric Imagery, S. Chakrabarti (ed.), Proc. SPIE, vol. 1744, 1992, p. 40. Also submitted to Optical Science.

McEntire, R.W., and Mitchell, D.G.: "Instrumentation for Global Magnetospheric Imaging Via Energetic Neutral Atoms." Solar System Plasma Physics, Geophys. Monogr. Ser., vol. 54, J. Burch and J. Waite (eds.), AGU, Washington, DC, 1989.

Meier, R.R.: "Ultraviolet Spectroscopy and Remote Sensing of the Upper Atmosphere." Space Sci. Rev., vol. 59, 1991, p. 1.

Moore, K.R., McComas, D.J., Funsten, H.O., and Thomsen, M.F.: "Low Energy Neutral Atoms in the Earth's Magnetosphere Modeling." Instrumentation for Magnetospheric Imagery, S. Chakrabarti (ed.), Proc. SPIE, 1744, 1992, p. 51. Also submitted to Optical Science.

Rairden, R.L., Frank, L.A., and Craven, J.D.: "Geocoronal Imaging With Dynamics Explorer." J. Geophys. Res., vol. 91, 1986, p. 13613.

Roelof, E.C.: "Energetic Neutral Atom Image of a Storm-Time Ring Current." Geophys. Res. Lett., vol. 14, 1987, p. 652.

Roelof, E.C.: "Remote Sensing of the Ring Current Using Energetic Neutral Atoms." Adv. Space Res., vol. 9, No. 12, 1989, p. 195.

Roelof, E.C., and Williams, D.J.: "The Terrestrial Ring Current: From In Situ Measurements to Global Images Using Energetic Neutral Atoms." Johns Hopkins APL Tech. Dig. 9, 1988, p. 144.

Roelof, E.C., and Williams, D.J.: "Update on Global Imaging Using Energetic Neutral Atoms." Johns Hopkins APL Tech. Dig. 11, 1990, p. 72.

Roelof, E.C., Mitchell, D.G., and Williams, D.J.: "Energetic Neutral Atoms (E = 50 keV) From the Ring Current: IMP 7/8 and ISEE 1." J. Geophys. Res., vol. 90, 1985, p. 10991.

Roelof, E.C., Mauk, B.H., and Meier, R.R.: Instrument Requirements for Imaging the Magnetosphere in Extreme-Ultraviolet and Energetic Neutral Atoms Derived From Computer-Simulated Images." Instrumentation for Magnetospheric Imagery, S. Chakrabarti (ed.), Proc. SPIE, vol. 1744, 1992, p. 19. Also submitted to Optical Science.

Roelof, E.C., Mauk, B.H., Meier, R.E., Moore, K.R., and Wolf, R.A.: "Simulations of EUV and ENA Magnetospheric Images Based on the Rice Convection Model." Instrumentation for Magnetospheric Imagery, S. Chakrabarti (ed.), Proc. SPIE, vol. 2008, 1993, pp. 202–213.

Roelof, E.C., Mauk, B.H., Chase, C.J., Mitchell, D.G., Williams, D.J., Sussman, D.W., Hobson, L.J., Wolf, R.A., and Spiro, R.W.: "Energetic Neutral Atom Images of a Geomagnetic Storm: A Computer-Simulated Visualization." JHU/APL Video, January 1994.

Weller, C.S., and Meier, R.R.: "First Satellite Observations of the He^+ 304-Å Radiation and Its Interpretation." J. Geophys. Res., vol, 79, 1974, p. 1572.

Williams, D.J.: "Why We Need Global Observations." Magnetospheric Physics, Plenum, New York, B. Hultqvist and C.G. Falthammer (eds.), 1990, p. 83.

Williams, D.J.: "Global Observations: A Future Research Thrust in Auroral and Magnetospheric Research." Auroral Physics, C.-I. Meng, M.J. Rycroft, and L.A. Frank (eds.), Cambridge University Press, 1991, pp. 449–456.

Williams, D.J., Roelof, E.C., and Mitchell, D.G.: Global Magnetospheric Imaging." Rev. Geophys., vol. 30, No. 3, 1992, p. 183.

Energetic Neutral Atom Imaging

Amsif, A., Dandouras, J., and Roelof, E.C.: "Modeling the Production of Energetic Neutral Atoms in Titan's Exosphere." J. Geophys. Res., submitted 1995.

Chase, C.J., and Roelof, E.C.: "Extracting Evolving Structures From Global Magnetospheric Images Via Model Fitting and Video Visualization." Johns Hopkins APL Tech. Dig, 16, in press, 1995.

Cheng, A.F., Keath, E.P., Krimigis, S.M., Mauk, B.H., McEntire, R.W., Mitchell, D.G., Roelof, E.C., and Williams, D.J.: "Imaging Neutral Particle Detector." Remote Sensing Reviews, vol. 8, 1993, p. 101.

Curtis, C.C., and Hsieh, K.-C.: "Remote Sensing of Planetary Magnetosphere: Imaging Via Energetic Neutral Atoms." Solar System Plasma Physics, J.H. Waite, Jr., J.L. Burch, and R.L. Moore (eds.), Geophys. Monogr. Ser., No. 54, 247-252, AGU, Washington, DC, 1989.

Frank, L.A., Sigwarth, J.B., Williams, D.J., Roelof, E.C., Mitchell, D.G., Gold, R.E., Keath, E.P., Mauk, B.H., Meng, C.-I., Carpenter, D.L., Hultqvist, B.K., Lundin, R.N., Siscoe, G.L., Wolf, R.A., Gorney, D.J., Schulz, M., McComas, D.J., Funsten, H.O., Moore, K.R., Smith, B.W., Craven, J.D., Chiu, Y.T., Meier, R.R., and Seely, J.F.: "Imagers for the Magnetosphere, Aurora, and Plasmasphere." Optical Engr., vol. 33, 1994, p. 391.

Funsten, H.O., McComas, D.J., and Barraclough, B.L.: "Thickness Uniformity and Pinhole Density Analysis of Thin Carbon Foils Using keV Ions." Nuclear Instruments and Methods in Physics Research, vol. B66, 1992, p. 470.

Funsten, H.O., Barraclough, B.L., and McComas, D.J.: Pinhole Detection in Thin Foils Used in Space Plasma Diagnostic Instrumentation." Rev. Sci. Inst., vol. 63, 1992, p. 4741.

Funsten, H.O., McComas, D.J., and Barraclough, B.L.: "Application of Thin Foils in Low Energy Neutral Atom Detection." Instrumentation for Magnetospheric Imagery, SPIE Proc., vol. 1744, 1992, p. 62.

Funsten, H.O., Barraclough, B.L., and McComas, D.J.: "Shell Effects Observed in Exit Charge State Distributions of 1–30 keV Atomic Projectiles Transiting Ultra-Thin Carbon Foils." Nuc. Inst. and Meth., vol. B80/81, 1993, p. 49.

Funsten, H.O., McComas, D.J., and Scime, E.E: "Low Energy Neutral Atom Imaging Techniques." Instrumentation for Magnetospheric Imagery II, SPIE Proc., vol. 2008, 1993, p. 93.

Funsten, H.O., McComas, D.J., and Barraclough, B.L.: "Ultrathin Foils Used for Low Energy Neutral Atom Imaging of Planetary Magnetospheres." Optical Engineering, vol. 32, 1993, p. 3090.

Funsten, H.O., McComas, D.J., Moore, K.R., Scime, E.E., and Thomsen, M.F.: "Imaging of Magnetospheric Dynamics Using Low Energy Neutral Atom Detection." Solar System Plasmas in Space and Time, Geophys. Monogr. Ser., vol. 84, AGU, Washington, DC, 1994, p. 275.

Funsten, H.O., Barraclough, B.L., and McComas, D.J.: "Interaction of Slow H, H_2, and H_3 in Thin Foils." Nuc. Inst. Meth. in Phys. Res. B, vol. 20, 1994, p. 24.

Funsten, H.O., McComas, D.J., and Scime, E.E.: "Comparative Study of Low Energy Neutral Atom Imaging Techniques." Optical Engineering, vol. 33, 1994, p. 349.

Ghielmetti, A.G., Shelley, E.G., Fuselier, S.A., Herrero, F., Smith, M.F., Wurz, P., Bochsler, P., and Stephen, T.: "A Mass Spectrograph for Imaging Low Energy Neutral Atoms." Proc. SPIE, vol. 2008, 1993, p. 362.

Ghielmetti, A.G., Shelley, E.G., Fuselier, S.A., Herrero, F., Smith, M.F., Wurz, P., Bochsler, P., and Stephen, T.: "A Mass Spectrograph for Imaging Low Energy Neutral Atoms." Optical Engineering, vol. 33, 1993, p. 362.

Herrero, F.A., and Smith, M.F.: "Imager of Low Energy Neutral Atoms (ILENA): Imaging Neutrals From the Magnetosphere at Energies Below 20 keV." Instrumentation for Magnetospheric Imagery, Proc. SPIE, vol. 1744, 1992

Hesse, M., Smith, M.F., Herrero, F., Ghielmetti, A.G., Shelley, E.G., Wurz, P., Bochsler, P., Gallagher, D.L., Moore, T.E., and Stephen, T.: "Imaging Ion Outflow in the High-Latitude Magnetosphere Using Low-Energy Neutral Atoms." Proc. SPIE, vol. 2008, 1993, p. 83.

Hesse, M., Smith, M.F., Herrero, F., Ghielmetti, A.G., Shelley, E.G., Wurz, P., Bochsler, P., Gallagher, D.L., Moore, T.E., and Stephen, T.: "Imaging Ion Outflow in the High-Latitude Magnetosphere Using Low-Energy Neutral Atoms." Optical Engineering, vol. 32, 1993, p. 3153.

Hsieh, K.-C., and Curtis, C.C.: "A Model for the Spatial and Energy Distributions of Energetic Neutral Atoms Produced Within the Saturn/Titan Plasma System." Geophys. Res. Lett., vol. 15, 1988, p. 772.

Hsieh, K.-C., and Curtis, C.C.: "Remote Sensing of Planetary Magnetospheres: Mass and Energy Analysis of Energetic Neutral Atoms." Solar System Plasma Physics, J.H. Waite, Jr., J.L. Burch, and R.L. Moore (eds.), Geophys. Monogr. Ser., No. 54, AGU, Washington, DC, 1989, p. 159.

Hsieh, K.C., Curtis, C.C., Fan, C.-Y., and Gruntmann, M.A.: "Techniques for the Remote Sensing of Space Plasma in the Heliosphere Via Energetic Neutral Atoms: A Review." Solar Wind Seven, Proc. Third COSPAR Colloquium, E. Marsch and R. Schwenn (eds.), Pergamon Press, Oxford, 1992, pp. 357–364.

Hsieh, K.C., Shih, K.L., McComas, D.J., Wu, S.T., and Wu, C.C.: "Forecasting the Arrival of Fast Coronal Mass Ejecta at Earth by the Detection of 2–20 keV Neutral Atoms." Instrumentation for Magnetospheric Imagery, SPIE Proc., vol. 1744, 1992, p. 72.

Keath, E.P., Andrews, G.B., Mauk, B.H., Mitchell, D.G., and Williams, D.J.: "Instrumentation for Energetic Neutral Atom Imaging of Magnetospheres." Solar System Plasma Physics, Geophys. Monogr. Ser., vol. 54, AGU, Washington, DC, 1989, p. 165.

McComas, D.J., Barraclough, B.L., Elphic, R.C., Funsten, H.O. III, and Thomsen, M.F.: "Magnetospheric Imaging With Low Energy Neutral Atoms." Proceedings of the National Academy of Sciences, USA, vol. 88, 1991, p. 9589.

McComas, D.J., Funsten, H.O., Gosling, J.T., Moore, K.R., and Thomsen, M.F.: "Low Energy Neutral Atom Imaging." Instrumentation for Magnetospheric Imagery, SPIE Proc., vol. 1744, 1992, p. 40.

McComas, D.J., Funsten, H.O., Gosling, J.T., Moore, K.R., Scime, E.E., and Thomsen, M.F.: "Fundamentals of Low Energy Neutral Atom Imaging." Optical Engineering, vol. 33, 1994, p. 335.

McEntire, R.W., and Mitchell, D.G.: "Instrumentation for Global Magnetospheric Imaging Via Energetic Neutral Atoms." Solar System Plasma Physics, J.H. Waite, Jr., J.L. Burch, and R.L. Moore (eds.), Geophys. Monogr. Ser., No. 54, AGU, Washington, DC, 1989, p. 69.

Mitchell, D.G., Cheng, A.F., Krimigis, S.M., Keath, E.P., Jaskulek, S.E., Mauk, B.H., McEntire, R.W., Roelof, E.C., Williams, D.J., Hsieh, K.C., and Drake, V.A.: "INCA, the Ion Neutral Camera for Energetic Neutral Atom Imaging of the Saturnian Magnetosphere." Optical Engr., vol. 32, 1993, p. 3096.

Moore, K.R., McComas, D.J., Funsten, H.O., and Thomsen, M.F.: "Low Energy Neutral Atoms in the Earth's Magnetosphere: Modeling." Instrumentation for Magnetospheric Imagery, SPIE Proc., vol. 1744, 1992, p. 51.

Moore, K.R., Funsten, H.O., McComas, D.J., Scime, E.E., and Thomsen, M.F.: "Terrestrial Magnetospheric Imaging: Numerical Modeling of Low Energy Neutral Atoms." Instrumentation for Magnetospheric Imagery II, SPIE Proc., vol. 2008, 1993, p. 190.

Moore, K.R., Scime, E.E., Funsten, H.O., McComas, D.J., and Thomsen, M.F.: "Low Energy Neutral Atom Emission From the Earth's Magnetosphere." Optical Engineering, vol. 33, 1994, p. 342.

Orsini, S., Candidi, M., Jaggi, M., Hsieh, K.-C., Curtis, C.C., Hudor, A.M., Livi, S., Wilken, B., Daglis, I.A., Flamini, E., Negri, B., Tinsley, B.A., and Gruntman, M.A.: "Proposal of an Italian Experiment for the Mission SAC-B—ISENA: Imaging Particle Spectrometer for Energetic Neutral Atoms." Instrumentation for Magnetospheric Imagery, S. Chakrabarti (ed.), Proc. SPIE, vol. 1744, 1992, p. 91–101.

Orsini, S., Daglis, I.A., Candidi, M., Hsieh, K.-C., Livi, S., and Wilken, B.: "Model Calculation of Energetic Neutral Atoms Precipitation at Low Altitudes." J. Geophys. Res., vol. 99, 1994,. p. 13489.

Rairden, R.L., Frank, L.A., and Craven, J.D.: "Geocoronal Imaging With Dynamics Explorer." J. Geophys. Res, vol. 91, 1986, p. 13613.

Roelof, E.C.: "Energetic Neutral Atom Image of a Storm-Time Ring Current." Geophys. Res. Lett., vol. 14, 1987, p. 652.

Roelof, E.C.: "Remote Sensing of the Ring Current Using Energetic Neutral Atoms."Adv. Space Res., vol. 9, No. 12, 1989, p. 195.

Roelof, E.C.: "Imaging Heliospheric Shocks Using Energetic Neutral Atoms." Solar Wind Seven, Proc. Third COSPAR Colloquium, E. Marsch and R. Schwenn (eds.), Pergamon Press, Oxford, 1992, pp. 385–390.

Roelof, E.C.: "Energetic Neutral Atom Imaging of Trapped Ion Dynamics." Proceedings of the Taos Workshop on the Earth's Trapped Particle Environment, submitted, 1995.

Roelof, E.C., and Williams, D.J.: "The Terrestrial Ring Current: From In Situ Measurements to Global Images Using Energetic Neutral Atoms." Johns Hopkins APL Tech. Dig., vol. 9, 1988, p. 144.

Roelof, E.C., and Williams, D.J.: "Update on Global Imaging Using Energetic Neutral Atoms." Johns Hopkins APL Tech. Dig., vol. 11, 1990, p. 72.

Roelof, E.C., Mitchell, D.G., and Williams, D.J.: "Energetic Neutral Atoms (E ~ 50 keV) From the Ring Current: IMP 7/8 and ISEE 1." J. Geophys. Res., vol. 90, 1985, p. 10991.

Roelof, E.C., Mauk, B.H., and Meier, R.R.: "Instrument Requirements for Imaging the Magnetosphere in Extreme-Ultraviolet and Energetic Neutral Atoms Derived From Computer-Simulated Images." Instrumentation for Magnetospheric Imagery, Proc. SPIE, S. Chakrabarti (ed.), vol. 1744, 1992, pp. 19–30.

Roelof, E.C., Mauk, B.H., Meier, R.R., Moore, K.R., and Wolf, R.A.: "Simulations of EUV and ENA Magnetospheric Images Based on the Rice Convection Model." Instrumentation for Magnetospheric Imagery II, Proc. SPIE, S. Chakrabarti (ed.), vol. 2008, 1993, p. 202–213.

Scime, E.E., Funsten, H.O., McComas, D.J., Moore, K.R., and Gruntman, M.: "Advances in Low Energy Neutral Atom Imaging Techniques." Instrumentation for Magnetospheric Imagery II, SPIE Proc., vol. 2008, 1993, p. 74.

Scime, E.E., McComas, D.J., Anderson, E.H., and Schattenburg, M.L.: "Extreme Ultraviolet Polarization and Filtering With Gold Transmission Gratings." Submitted to Applied Optics, 1993.

Scime, E.E., Funsten, H.O., McComas, D.J., Moore, K.R., and Gruntman, M.A.: "A Novel Low Energy Neutral Atom Imaging Technique." Optical Engineering, vol. 33, 1994, p. 357.

Scime, E.E., Funsten, H.O., McComas, D.J., and Hokin, S.: "Three Dimensional Neutral Atom Imaging of Tokamak Plasmas." Submitted to Rev. Sci. Inst., 1994.

Smith, M.F., Herrero, F., Hesse, M., Baker, D.N., Bochsler, P., Wurz, P., Balsiger, H., Chakrabarti, S., Erickson, G., Cotton, D., Stephen, T.S., Jamar, C., Gerard, J.C., Fuselier, S.A., Ghielmetti, A.G., Mende, S.B., Peterson, W.K., Shelley, E.G., Vondrak, R.R., Gallagher, D.L., Moore, T.E., Pollock, C., Arnoldy, R., Lockwood, M., and Gladstone, R.: "The High-Latitude Ion Transport and Energetics (HI-LITE) Explorer: A Mission to Investigate Ion Outflow From the High-Latitude Ionosphere." Proc. SPIE, vol. 2008, 1993, p. 40.

Voss, H.D., Mobilia, J., Collin, H.L., and Imhof, W.L.: "Satellite Observations and Instrumentation for Imaging Energetic Neutral Atoms." Instrumentation for Magnetospheric Imagery, Proc. SPIE, S. Chakrabarti (ed.), vol. 1744, 1992, pp. 79–90.

Williams, D.J.: "Why We Need Global Observations." Magnetospheric Physics, Plenum Press, New York, B. Hultqvist and C.G. Falthammer (eds.), 1990, p. 83.

Williams, D.J.: "Global Observations: A Future Research Thrust in Auroral and Magnetospheric Research." Auroral Physics, Cambridge University Press, C.-I. Meng, M.J. Rycroft, and L.A. Frank (eds.), 1991, pp. 449–456.

Williams, D.J., Roelof, E.C., and Mitchell, D.G.: "Global Magnetospheric Imaging." Rev. Geophys., vol. 30, 1992, p. 183.

Wurz, P., Bochsler, P., Ghielmetti, A.G., Shelley, E.G., Herrero, F., and Smith, M.F.: "Concept for the HI-LITE Neutral Atom Imaging Instrument." Proc. Symposium on Surface Science, P. Varga and G. Betz (eds.), in press, 1994.

Wurz, P., Bochsler, P., Ghielmetti, A.G., Shelley, E.G., Herrero, F., and Smith, M.F.: "Remote Imaging of Ion Distribution Using Low Energy Neutral Atoms." Helv. Phys. Acta, in press, 1994.

Wurz, P., Aellig, M.R., Bochsler, P., Ghielmetti, A.G., Shelley, E.G., Fuselier, S., Herrero, F., Smith M.F., and Stephen, T.S.: "Neutral Atom Imaging Mass Spectrograph." Optical Engineering, submitted, 1994.

Plasmaspheric Imaging

Bertaux J.-L., Goutail, F., and Kockarts, G.: "Observations of Lyman-α Emissions of Hydrogen and Deuterium." Science, vol. 225, 1984, p. 174.

Bertaux J.-L., le Texier, H., Goutail, F., Lallement, R., and Kockarts, G.: "Lyman-α Observations of Geocoronal and Interplanetary Hydrogen From Spacelab 1: Exospheric Temperature and Density and Hot Emission." Ann. Geophys., vol. 7, 1989, p. 549.

Carpenter, D.L.: "The Earth's Plasmasphere Awaits Rediscovery." EOS, Transactions, American Geophysical Union, in press, 1995.

Carpenter, D.L., and Park, C.G.: "On What Ionospheric Workers Should Know About the Plasmapause-Plasmasphere." Rev. Geophys. Space Physics, vol. 11, 1973, p. 133.

Carpenter, D.L., and Anderson, R.R.: "An ISEE/Whistler Model of Equatorial Electron Density in the Magnetosphere." J. Geophys. Res., vol. 97, 1992, p. 1097.

Chakrabarti S., Paresce, F., Bowyer, S., Chiu, Y.T., and Aikin, A.: "Plasmaspheric Helium Ion Distribution From Satellite Observations of He II 304Å." Geophys. Res. Lett., vol. 9, 1082, p. 151.

Chappell, C.R., Moore, T.E., and Waite, J.H. Jr.: "The Ionosphere as a Fully Adequate Source of Plasma for the Earth's Magnetosphere." J. Geophys. Res., vol. 92, 1987, p. 5896.

Chase, C.J., and Roelof, E.C.: "Extracting Evolving Structures From Global Magnetospheric Images Via Model Fitting and Video Visualization." Johns Hopkins APL Tech. Dig., vol. 16, in press, 1995.

Chiu, Y.T., Robinson, R.M., Swenson, G.R., Chakrabarti, S., and Evans, D.S.: "Imaging the Outflow of Ionospheric Ions Into the Magnetosphere." Nature, vol. 322, 1986, p. 441.

Chiu, Y.T., Collin, R.M., Chakrabarti, S., and Gladstone, G.R.: "Magnetospheric and Exospheric Imaging in the Extreme Ultraviolet." Geophys. Res. Lett.., vol. 17, 1990, p. 267.

Frank, L.A., Williams, D.J., and Roelof, E.C.: "Imagers for the Magnetosphere, Aurora and Plasmasphere (IMAP)." Instrumentation for Magnetospheric Imagery II, Proc. SPIE, S. Chakrabarti (ed.), 1993, p. 2008.

Frank, L.A., Sigwarth, J.B., Williams, D.J., Roelof, E.C., Mitchell, D.G., Gold, R.E., Keath, E.P., Mauk, B.H., Meng, C.-I., Carpenter, D.L., Hultqvist, B.K., Lundin, R.N., Siscoe, G.L., Wolf, R.A., Gorney, D.J., Schulz, M., McComas, D.J., Funsten, H.O., Moore, K.R., Smith, B.W., Craven, J.D., Chiu, Y.T., Meier, R.R., and Seely, J.F.: "Imagers for the Magnetosphere, Aurora, and Plasmasphere." Optical Engr., vol. 33, 1994, p. 391.

Garrido, D.E., Smith, R.W., Swift, D.F., and Akasofu, S.-I.: "Imaging the Earth's Magnetosphere: Effects of Plasma Flow and Temperature." Planet. Space Sci., vol. 39, 1991, p. 1559.

Gladstone, G.R.: "Simulated Images of the Magnetosphere." Instrumentation for Magnetospheric Imagery, Proc. SPIE, S. Chakrabarti (ed.), vol. 1744, 1992, p. 171.

Horowitz, J.L., Comfort, R.H, and Chappell, C.R.: "A Statistical Characterization of Plasmasphere Density Structure and Boundary Locations." J. Geophys. Res., vol. 95, 1990, p. 7937.

Johnson, C.Y., Young, J.M., and Holmes, J.C.: "Magnetoglow—A New Geophysical Resource." Science, vol. 171, 1971, p. 379.

Meier, R.R.: "The Scattering Rate of Solar 834 Å Radiation by Magnetospheric O^+ and O^{++}." Geophys. Res. Lett., vol. 17, 1990, p. 1613.

Meier, R.R.: "Ultraviolet Spectroscopy and Remote Sensing of the Upper Atmosphere." Space Sci. Rev., vol. 59, 1991, p. 1.

Meier, R.R., and Weller, C.S.: "EUV Resonance Radiation From Helium Atoms and Ions in the Geocorona." J. Geophys. Res., vol. 77, 1972, p. 1190.

Murphy, D.L., and Chiu, Y.T.: "Effects of Doppler Shifts and Source Perspectives on Extreme Ultraviolet Images of Ion Populations Moving in the Inner Magnetosphere." Geophys. Res. Lett., submitted 1993.

Paresce, F., Bowyer, C.S., and Kumar, S.: "On the Distribution of He^+ in the Plasmasphere From Observations of Resonantly Scattered HeII 304-Å Radiation." J. Geophys. Res., vol. 79, 1974, p. 174.

Press, W.H., Flannery, B.P., Teukolsky, S.A., and Vetterling, W.T.: "Numerical Recipes." Cambridge University Press, Cambridge, 1989.

Rairden, R.L., Frank, L.A., and Craven, J.D.: "Geocoronal Imaging With Dynamics Explorer." J. Geophys. Res, vol. 91, 1986, p. 13613.

Roberts, W.H., Jr., Horwitz, J.L., Comfort, R.H., Chappell, C.R., Waite, J.H., Jr., and Green, J.L.: "Heavy Ion Density Enhancements in the Outer Plasmasphere." J. Geophys. Res., vol. 92, 1987, p. 13499.

Roelof, E.C., Mauk, B.H., and Meier, R.R.: "Instrument Requirements for Imaging the Magnetosphere in Extreme-Ultraviolet and Energetic Neutral Atoms Derived From Computer-Simulated Images." Instrumentation for Magnetospheric Imagery, Proc. SPIE, S. Chakrabarti (ed.), vol. 1744, 1992, p. 19.

Roelof, E.C., Mauk, B.H., Meier, R.R., Moore, K.R., and Wolf, R.A.: "Simulations of EUV and ENA Magnetospheric Images Based on the Rice Convection Model." Instrumentation for Magnetospheric Imagery II, Proc. SPIE, S. Chakrabarti (ed.), vol. 2008, 1993, pp. 202–213.

Swift, D.W., Smith, R.W. and Akasofu, S.-I.: "Imaging the Earth's Magnetosphere." Planet. Space. Sci., vol. 37, 1989, p. 379.

Weller, C.S., and Meier, R.R.: "First Satellite Observations of the He^+ 304-Å Radiation and Its Interpretation." J. Geophys. Res., vol. 79, 1974, p. 1572.

Williams, D.J.: "Why We Need Global Observations." Magnetospheric Physics, B. Hultqvist and C.G. Falthammer (eds.), Plenum Press, New York, 1990, p. 83.

Williams, D.J.: "Global Observations: A Future Research Thrust in Auroral and Magnetospheric Research." Auroral Physics, C.-I. Meng, M.J. Rycroft (eds.), and L.A. Frank, Cambridge University Press, 1991, pp. 449–456.

Williams, D.J., Roelof, E.C., and Mitchell, D.G.: "Global Magnetospheric Imaging." Rev. Geophys., vol. 30, 1992, p. 183.

Wolf, R.A., Spiro, R.W., and Rich, F.J.: "Extension of the Rice Convection Model Into the High-Latitude Ionosphere." J. Atm. Terrest. Phys., vol. 53, 1991, p. 817.

Auroral and Geocoronal Imaging

Akasofu, S.I.: "Physics of Magnetospheric Substorms." D. Reidel, Hingham, MA, 1977.

Anger, C.D., Sawchuk, W., and Shepher, G.G.: "Polar Cap Optical Aurora Seen for ISIS2." Magnetospheric Physics, B.M. McCormac (ed.), D. Reidel, Dordrecht, Holland, 1974, p. 357.

Chamberlain, J.W.: "Physics of the Aurora and Airglow." Academic Press, New York, 1961.

Chamberlain, J.W., and Hunten, D.M.: "Theory of Planetary Atmospheres." Academic Press, New York, 1987.

Craven, J.D., and Frank, L.A.: "Latitudinal Motions of the Aurora During Substorms." J. Geophys. Res., vol. 92, 1987, p. 4565.

Frank, L.A., Craven, J.D., Gurnett, D.A., Shawhan, S.D., Weimer, D.R., Burch, J.L., Winningham, J.D., Chappell, C.R., Waite, J.H., Heelis, R.A., Maynard, N.C., Sugiura, M., Peterson, W.K., and Shelley, E.G.: "The Theta Aurora." J. Geophys. Res., vol. 91, 1986, p. 3177.

Frank, L.A., Sigwarth, J.B., Williams, D.J., Roelof, E.C., Mitchell, D.G., Gold, R.E., Keath, E.P., Mauk, B.H., Meng, C.-I., Carpenter, D.L., Hultqvist, B.K., Lundin, R.N., Siscoe, G.L., Wolf, R.A., Gorney, D.J., Schulz, M., McComas, D.J., Funsten, H.O., Moore, K.R., Smith, B.W., Craven, J.D., Chiu, Y.T., Meier, R.R., and Seely, J.F.: "Imagers for the Magnetosphere, Aurora, and Plasmasphere." Optical Engr., vol. 33, 1994, p. 391.

Hodges, R.R., Jr., Rohrbaugh, R.P., and Tinsley, B.A.: "The Effect of the Charge Exchange Source on the Velocity and 'Temperature' Distributions and Their Anisotropies in the Earth's Exosphere." J. Geophys. Res., vol. 86, 1981, p. 6917.

Jones, A.V.: "Aurora." D. Reidel, Dordrecht, Holland, 1974.

Kaneda, E., and Yamamoto, T.: "Auroral Substorms Observed by UV Imager on Akebono." Magnetospheric Substorms, Geophys. Monogr. Ser., vol. 64, J.R. Kan, T.A. Potemra, S. Kokubun, and T. Iijima (eds.), AGU, Washington, DC, 1991, p. 235.

Mange, P., and Meier, R.R.: "Ogo 3 Observations of the Lyman-α Intensity and the Hydrogen Concentration Beyond 5 R_E." J. Geophys. Res., vol. 75, 1970, p. 1837.

Meng, C.I., and Huffman, R.E.: "Ultraviolet Imaging From Space of the Aurora Under Full Sunlight." Geophys. Res. Lett., vol. 11, 1984, p. 315.

Murphree, J.S., Cogger, L.L., Anger, C.D., Wallis, D.D., and Shepherd, G.G.: "Oval Intensifications Associated With Polar Arcs." Geophys. Res. Lett., vol. 14, 1987, p. 403.

Omholt, A.: "The Optical Aurora." Springer Verlag, Berlin, 1971.

Rairden, R.L., Frank, L.A., and Craven, J.D.: "Geocoronal Imaging With Dynamics Explorer." J. Geophys. Res, vol. 91, 1986, p. 13613.

Rogers, E.H., Nelson, D.F., and Savage, R.C.: "Auroral Photography From a Satellite." Science, vol. 183, 1974, p. 951.

Rostoker, G., Jones, A.V., Gattinger, R.L., Anger, C.D., and Murphree, J.S.: "The Development of the Substorm Expansive Phase: The 'Eye' of the Substorm." Geophys. Res. Lett., vol. 14, 1987, p. 399.

Strickland, D.J., Jasperse, J.R., and Whalen, J.A.: "Dependence of Auroral FUV Emissions on the Incident Electron Spectrum and Neutral Atmosphere." J. Geophys. Res., vol. 88, 1983, p. 8051.

Thomas, G.E., and Bohlin, R.C.: "Lyman Alpha Measurements of Neutral Hydrogen in the Outer Geocorona and in Interplanetary Space." J. Geophys. Res., vol. 77, 1972, p. 2752.

Tinsley, B.A.: "Hydrogen in the Upper Atmosphere." Fundamentals of Cosmic Physics, vol. 1, Gordon and Breach, New York, 1974, p. 201.

Weimer, D.R., Craven, J.D., Frank, L.A., Hanson, W.B., Maynard, N.C., Hoffman, R.A., and Slavin, J.A.: "Satellite Measurements Through the Center of a Substorm Surge." J. Geophys. Res., vol. 99, 1994, p. 23639.

Williams, D.J.: "Why We Need Global Observations." Magnetospheric Physics, B. Hultqvist and C.G. Falthammer (eds.), Plenum Press, New York, 1990, p. 83.

Williams, D.J.: "Global Observations: A Future Research Thrust in Auroral and Magnetospheric Research." Auroral Physics, C.-I. Meng, M.J. Rycroft, and L.A. Frank (eds.), Cambridge University Press, 1991, p. 449–456.

Williams, D.J., Roelof, E.C., and Mitchell, D.G.: "Global Magnetospheric Imaging." Rev. Geophys., vol. 30, 1992, p. 183.

X-Ray Imaging

Miller, K.L., and Vondrak, R.R.: "A High-Latitude Phenomenological Model of Auroral Precipitation and Ionospheric Effects." Radio Sci., vol. 20, 1985, p. 431.

Mizera, P.F., Gorney, D.J., and Roeder, J.L.: "Auroral X-Ray Images From DMSP-F6." Geophys. Res. Lett., vol. 11, 1984, p. 255.

Voss, H.D., Reagan, J.B., Imhoff, W.L., Murray, D.O., Simpson, D.A., Cauffman, D.P., and Bakke, J.C.: "Low Temperature Characteristics of Solid State Detectors for Energetic X-Ray Ion and Electron Spectrometers." IEEE Nucl. Sci., vol. 29, 1982, p. 164.

Radio Plasma Sounding

Calvert, W., McAfee, J.R., Norton, R.B., Thompson, T.L., Warnock, J.M., and Whipple, E.C.: "A Plasmaspheric Sounder Satellite." NOAA Technical Report ERL 242-AL8, ERL, NOAA, Boulder, CO, 1972.

Calvert, W.: "The Detectability of Ducted Echoes in the Magnetosphere." J. Geophys. Res., vol. 86, 1981, pp. 1609–1612.

Calvert, W., Benson, R.F., Carpenter, D.L., Fung, S.F., Gallagher, D., Green, J.L., Reiff, P.H., Reinisch, B.W., Smith, M., and Taylor, W.W.L.: "The Feasibility of Radio Sounding of the Magnetosphere." Submitted to Radio Science, 1994.

Franklin, C.A., and MaClean, M.A.: "The Design of Swept-Frequency Topside Sounders." Proc. Inst. Elec. Engrs., London, vol. 57, 1969, pp. 897–929.

Fung, S.F., Green, J.L., Benson, R.F., Calvert, W., Carpenter, D., Gallagher, D., Reiff, P.H., Reinisch, B.W., Smith, M.F., and Taylor, W.W.L.: "Probing the Magnetopause and Boundary Layers by the Radio Sounding Technique." Submitted to J. Geophys. Res., 1994.

Green, J.L., and Fung, S.F.: "Radio Sounding of the Magnetosphere From a Lunar-Based VLF Array." Adv. Space Res., vol. 14, No. 6, 1994, p. 217.

Green, J.L., Benson, R.F., Calvert, W., Fung, S.F., Reiff, P.H., Reinisch, B.W., and Taylor, W.W.L.: "A Study of Radio Plasma Imaging for the Proposed IMI Mission." NSSDC Technical Publication, February 1993.

Green, J.L., Benson, R.F., Carpenter, D.L., Calvert, W., Fung, S.F., Gallagher, D., Reiff, P.H., Reinisch, B.W., Smith, M., and Taylor, W.W.L.: "Radio Sounding of the Magnetosphere." In preparation for submission to J. Geophys. Res., 1995.

Ondoh, T., Nakamura, Y., and Koseki, T.: "Feasibility Study of Plasmapause Sounding From a Geostationary Satellite." Space Sci. Instrum., vol. 4, 1978, pp. 57–71.

Reiff, P.H., Green, J.L., Benson, R.F., Carpenter, D., Calvert, W., Fung, S.F., Gallagher, D., Reinisch, B.W., Smith, M.F., and Taylor, W.W.L.: "Radio Imaging of the Magnetosphere." Feature article in EOS, vol. 75, 1994, pp. 129, 133, and 134.

Reiff, P.H., Green, J.L., Benson, R.F., Carpenter, D.L., Calvert, W., Fung, S.F., Gallagher, D., Omura, Y., Reinisch, B.W., Smith, M.F., and Taylor, W.W.L.: "Remote Sensing of Substorm Dynamics Via Radio Sounding." Proceedings of the Second International Conference on Substorms, J.R. Kan, J.D. Craven and S.-I. Akasofu (eds.), in press, 1995.

Reinisch, B.W.: "New Techniques in Ground-Based Ionospheric Sounding and Studies." Radio Science, vol. 21, No. 3, 1986, p. 331.

Reinisch, B.W., Haines, D.M., and Kuklinski, W.S.: "The New Portable Digisonde for Vertical and Oblique Sounding." AGARD Proceedings, vol. 502, 1992, pp. 11-1 to 11-11.

Previous Proposals

Calvert, W. et al.: "Proposed Mission for ISIS-C: Plasmaspheric Sounder." Communications Research Centre, Ottawa, Canada, proposal to NASA and the Canadian Space Agency, July 1969.

Calvert, W., McAfee, J.R., Norton, R.B., Thompson, T.L., Warnock, J.M., and Whipple, E.C.: "Satellite Radio Sounder to Study the Plasmasphere." Proposal submitted to NASA and the Canadian Space Agency for the ISIS-C Mission, April 1, 1970.

Calvert, W., Green, J.L., Fung, S.F., Smith, M.F., Benson, R.F., Carpenter, D.L., Reinisch, B.W., Reiff, P.H., and Taylor, W.W.L.: "Simulation of Radio Sounding of the Plasmasphere." Proposal submitted to MSFC for NRA 8-8, September, 1993.

Frank, L.A., Williams, D.J., Keath, E.P., Mitchell, D.G., Roelof, E.C., Craven, J.D., Meng, C.-I., Sigwarth, J.B., Hultqvist, B., Lundin, R., Roble, R.G., and Siscoe, G.L.: "Magnetospheric-Auroral Reconnaissance Imaging Explorer (MARIE)." Proposal to NASA for the MARIE small-class Explorer mission, July 1988.

Frank, L.A., Williams, D.J., Mitchell, D.G., Gold, R.E., Keath, E.P., Mauk, B.H., Roelof, E.C., McComas, D.J., Funsten, H.O., Moore, K.R., Sigwarth, J.B., Craven, J.D., Meng, C.I., Gorney, D.J., Chiu, Y.T., Meier, R.R., Seely, J.F., Schulz, M., Smith, B.W., Carpenter, D.L., Hultqvist, B.K., Lundin, R.N., Siscoe, G.L., and Wolf, R.A.: "Imagers for the Magnetosphere, Aurora and Plasmasphere (IMAP)." Proposal to NASA for the IMAP Small Class Explorer mission, January 1993.

Ghielmetti, A., Fuselier, S., Shelley, E., Osiecki, R., Smith, M.F., Herrero, F., Stephen, T., Bochsler, P., and Wurz, P.: "Surface Conversion Techniques of Low Energy Neutral Atom Imagers." Proposal submitted to NASA MSFC in response to NRA8-8 (proposal funded)

Green, J.L., Fung, S.F., Candey, R.M., and Aist-Sagara, L.: "Remote Sensing of the Magnetosphere by an Active Sounder." Proposal submitted in response to NASA Headquarters NRA 90-OSSA-11, July, 1990.

Hsieh, K.C., Curtis, C.C., Fan, C.Y., Tinsley, B.A., Thomas, G.E., Bell, A.E., Swanson, L.W., Ip, W.-H., Korth, A., and Richter, A.K.: "HELENA." Proposal to perform an in situ investigation of neutrals in geospace and the heliosphere on PPL and IPL of the OPEN mission, March 1980.

Reinisch, B.W., Haines, D.M., Benson, R.F., Fung, S.F., and Green, J.L.: "Instrument Definition of a Radio Sounder for Global Magnetospheric Imaging." Unsolicited proposal submitted to MSFC related to NRA 8-8, December 1993.

Reinisch, B.W., Haines, D.M., Benson, R.F., Fung, S.F., Green, J.L., Culvert, W., and Taylor, W.W.L.: "Sounder for Planetary Ionospheric Missions (SPIM)." Proposal submitted in response to NASA Headquarters NRA 94-OSS-11, October 1994.

Sauvaud, J.A., Bertaux, J.L., LeQuéau, D., Perraut, S., Prangé, R., Bougeret, J.L., Harvey, C.C., Lefeuvre, F., Villain, J.P., Rauch, J.L., Treilhou, J.P., Dandouras, Y., Jacquey, C., Rème, H., Lundin, R., Pellinen, R., Koskinen, H., Wilken, B., Korth, A., Livi, S., Büchner, J., Delcourt, D., Girard, L., Berthelier, J.J., Blanc, M., Lilensten, J., Sanahuja, B., Pedersen, A., Stadsnes, J., Bjordal, J., Galperin, Y.I., Cogger, L.L., Murphree, S., Williams, D.J., Roelof, E.C., Green, J.L., Benson, R.F., Fung, S.F., Calvert, W., Reinisch, B.W., Vondrak, R.R., Chenette, D., Broadfoot, A.L., Sandel, B.R., Parks, G.K., McCarthy, M., Reiff, P.H., and Taylor, W.W.L.: A Proposal to the European Space Agency for a MAGnetospheric Imaging Circumterrestrial Satellite (MAGICS), in response to the call for mission ideas issued 26th November 1992.

Smith, M.F., Slavin, J.A., Herrero, F., Hesse, M., Quinn, J., Ghielmetti, A., Stephen, T., Bochsler, P., Wurz, P., and Cravens, T.: "Development of a Low Energy Neutral Atom Imager for Planetary Missions." Proposal submitted to NASA in response to NRA 93-OSS-04.

Taylor, W.W.L., Burdick, B.J., and Reinisch, B.W.: "Signal Processing for Radio Plasma Imaging." Unsolicited proposal submitted to MSFC related to NRA 8-8, December, 1993.

Taylor, W.W.L., Green, J.L., Benson, R.F., and Fung, S.F.: "Radio Plasma Imaging/Sounding in the Magnetosphere." Proposal submitted in response to NASA Headquarters NRA 94-OSS-08, August, 1994.

Williams, D.J., Frank, L.A., Broadfoot, A.L., Imhoff, W.L., Mende, S.B., Hunten, D.M., Roble, R.G., and Siscoe, G.L.: "Images of Magnetosphere and Atmosphere: Global Effects (IMAGE)." Proposal to NASA for the IMAGE Explorer Mission Concept, July 1986.

ENHANCEMENT AND EXTENSIONS OF MI OBSERVATIONS

In the process of refining the scope of instrument and spacecraft resources required to achieve MI science objectives, the SDT has carefully considered a range of observations and instruments. The measurement set identified as core (ENA of ring current, EUV of plasmasphere, and FUV of aurora and geocorona) do not exhaust the list of important and valuable observations. It is hoped that improvements in technology and cost effective approaches to flight will allow the consideration of and possible inclusion of the measurements described in the following sections. The science return of MI would be increased thereby.

Proton Aurora

Because the MI instrumentation for ENA's is capable of providing images of the magnetospheric distributions of energetic protons, it would be very useful to enhance the mission scientific objectives by obtaining simultaneous images of the footprints of these distributions in the auroral ionosphere, i.e., the proton auroras. Together with the FUV auroral imager that is already included in the primary instrument set, this enhancing instrument could be used to establish the temporal and spatial relationships of the magnetospheric proton deposition into the atmosphere with those for the generally brighter emissions for electron precipitation. The availability of simultaneous images of the proton and electron auroras offers considerable information about the relationship of the magnetospheric proton distributions with the electrons that are associated with discrete arcs and diffuse auroras. Thus, images of proton auroras provide further closure concerning the effects of magnetospheric topology and dynamics on Earth's upper atmosphere.

The hydrogen emissions from the precipitation of energetic protons into the upper atmosphere are due to charge exchange with the neutral atmospheric atoms and subsequent emission from the excited energetic hydrogen atom. This atom is subsequently stripped of its electron, followed by another pickup of an electron in the charge exchange process, and the emission of another photon. This cycle of events is repeated with the result that approximately 10 to 100 photons of a given wavelength are emitted from the precipitation of a single magnetospheric proton. There are three emissions that are useful for imaging the proton auroras: the two Balmer lines Hα (656.3 nm) and Hβ (486.1 nm) and the Lyman-α emissions at 121.6 nm. The number of photons per incident proton is dependent on the proton energy. For example, about 20 Hα photons are emitted during the impact of a 30 keV proton (Eather, 1967). The typical intensities for a proton aurora are several hundred Rayleighs (R) or less. The intensities of Hβ are factors of 2 to 3 less than those of Hα. On the other hand, the efficiencies for the production of Lyman-α emissions are larger than those for Hα by factors of 5 to 10 (Edgar et al., 1973). Thus, the proton auroral intensities are in the range of several kilorayleighs (kR) for the Lyman-α emissions (Paresce et al., 1983; Ishimoto et al., 1989).

Because of the low intensities of the proton auroral emissions and/or the large background intensities, the images are most effectively gained in a "staring" mode, i.e., such that the camera field of view stares at the aurora in order to maximize its sensitivity relative to a spinscan image from a rotating spacecraft. Thus, a despun platform is required in order to obtain 50- to 100-km resolutions from the MI apogee position with frame repetition rates in the range of 1 min. Proton auroral imaging from a spinning platform will be significantly degraded with respect to these reasonable expectations because of the insufficiency of the counting statistics for a reasonably sized instrument. Imaging at the two visible wavelengths, Hα and Hβ, will not be possible for the sunlit atmosphere. This dayglow is much too intense for viewing the proton aurora. In the nightside atmosphere the nightglow is typically tens of R, but substantial backgrounds due to lunar and stellar illumination of the Earth's surface and cloud cover must be determined and subtracted. It is possible to obtain dayside images of the proton aurora at Lyman-α wavelengths. Such an imager must have sufficient spectral resolution to separate the resonantly scattered sunlight associated with the relatively cold geocoronal hydrogen from the Doppler-shifted emissions associated with the energetic precipitating protons. The required spectral resolution is in the range of 0.2 nm, the Doppler equivalent of

about 500 km/s at these wavelengths (Ishimoto et al., 1989). This spectral resolution will also be required to image the nightside proton auroras from the generally polar position of the MI apogee because the geocoronal intensities along the line of sight are in the range of several kR (Rairden et al., 1986). These restraints on the spectral resolution, together with the significant background, require that the instrument field of view stares at the aurora in order to achieve the above performance goals.

The mass and power estimates for a proton imager for Lyman-α wavelengths and with the appropriate spectral resolutions are 20 kg and 15 W, respectively. The dimensions, length, width, and height, are 50, 40, and 25 cm, respectively. Telemetry rates are in the range of 10 kb/s. A despun platform is required.

References

Eather, R.H. (1967): "Auroral Proton Precipitation and Hydrogen Emissions." Rev. Geophys. Space Phys., vol. 5, p. 207.

Edgar, B.C., Miles, W.T., and Green, A.E.S. (1973): "Energy Deposition of Protons in Molecular Nitrogen and Applications to Proton Auroral Phenomena." J. Geophys. Res., vol. 78, p. 6595.

Ishimoto, M., Meng, C.I., Romick, G.R., and Huffman, R.E. (1989): "Doppler Shift of Auroral Lyman Alpha Observed From a Satellite." Geophys. Res. Lett., vol. 16, p. 143.

Paresce, F., Chakrabarti, S., Bowyer, S., and Kimble, R. (1983): "The Extreme Ultraviolet Spectrum of Dayside and Nightside Aurorae: 8001400 Å." J. Geophys. Res., vol. 88, p. 4905.

Rairden, R.L., Frank, L.A., and Craven, J.D. (1986): "Geocoronal Imaging With Dynamics Explorer." J. Geophys. Res., vol. 91, p. 13613.

Auroral X Rays, X-Ray Imaging Cameras

In recent years, several space-based imagers have been developed to image the auroras in the x-ray wavelength region (Voss et al., 1983; Mizera et al., 1984). These x rays are bremsstrahlung x rays produced in the atmosphere from precipitated energetic electrons. The bremsstrahlung theory for x-ray production is well known, and the inversion of the measured energy x-ray spectra will directly yield information on the energy spectra of the primary electrons. This capability is important for Earth observations where there are more than one source of energetic electrons. Precipitated electrons come from both the ionosphere and the distant magnetosphere. These two sources accelerate electrons to different energies, <10 keV for the ionospheric and several hundred keV and even to relativistic energies for the magnetospheric sources.

X-ray measurements can distinguish these electron sources, and x-ray cameras are the only means for obtaining unambiguous information on the spatial and temporal properties of these electron sources. X-ray information is needed to quantify how much energy is precipitated and how currents flow in the ionosphere. X-ray measurements combined with global observations of magnetospheric morphology can considerably enhance the understanding of magnetospheric dynamics.

Tabulation of x-ray source strengths are made for incident electron spectra by assuming that x rays are isotropic in the downward hemisphere. For convenience, it is assumed that the precipitated energy spectrum is exponential in form. The results tabulated in the following are examples of what a PIXIE-like camera on Polar spacecraft would detect. The flux numbers are normalized per unit total electron energy flux (one erg per cm^2-s into the atmosphere). See also Miller and Vondrak (1985) who have computed the intensity of x-ray photons as a function of energy for different types of auroral energy spectral forms.

Electron e-folding energy (keV)	X-ray flux at 3 keV per (cm^2-sr-s-keV-erg)	Integral flux 3–30 keV per (cm^2-sr-s-erg)	Counts/second at 6 R_E per pixel per erg
1	1.1×10^2	1.1×10^2	0.23
2	5.3×10^2	6.7×10^2	1.35
5	1.2×10^3	2.6×10^3	5.18
10	1.4×10^3	5.0×10^3	10.13
20	1.2×10^3	7.1×10^3	14.6
50	7.8×10^2	9.0×10^3	18

This assumes that the average detection sensitivity for the camera is 45 percent for x rays ~3 to 30 keV, energy resolution is ~15 percent, camera has a focal length of ~20 cm, and the geometrical factor is 1.8×10^{-3} cm^2-sr per pixel. For PIXIE-like cameras that have 128 by 128 pixels, the expected integration times is ~10 to 1,000 s.

References

Miller, K.L., and Vondrak, R. R. (1985): "A High-Latitude Phenomenological Model of Auroral Precipitation and Ionospheric Effects." Radio Sci., vol. 20, p. 431.

Mizera, P.F., Gorney, D.J., and Roeder, J.L. (1984): "Auroral X-Ray Images From DMSP-F6." Geophys. Res. Lett., vol. 11, p. 255.

Voss, H.D., Reagan, J.B., Imhoff, W.L., Murray, D.O., Simpson, D.A., Cauffman, D.P., and Bakke, J.C. (1982): "Low Temperature Characteristics of Solid State Detectors for Energetic X-Ray Ion and Electron Spectrometers." IEEE Nucl. Sci., vol. 29, p. 164.

Plasmaspheric 834 Å Emission From O, O^+ 834 Å Imager

The O^+ ion is an important signature of the coupling between the ionosphere and the magnetosphere. Measurements of O^+ 834 Å emissions in the dayglow (Chakrabarti et al., 1983; Kumar et al., 1983; McCoy et al., 1985) demonstrated the utility of this spectral feature in characterizing the thermosphere and the ionosphere. Other measurements have suggested the tantalizing possibility of detecting upflowing O^+ ions near the auroral regions using the same emission (Chakrabarti et al., 1984; Chiu et al., 1986). The imaging of this emission in the normal sense appears to be difficult. On the other hand, important understanding of the global magnetospheric dynamics can be obtained by relating the thermosphere/ionosphere to the magnetosphere.

In the sunlit thermosphere and in the aurora, the O^+ emission is strong and peaks in the lower thermosphere. In the auroral region, where upward flow occurs, the O^+ density is expected to be high, but the column is short. Through the plasmasphere, the pathlength is long, but the density may be low. To overcome these conflicting scenarios, it is suggested that by co-adding to increase effective exposure time and by adjusting field-of-view constraints, important intensity profiles coupling the thermosphere to the magnetosphere can be obtained.

The technical difficulty in this wavelength region is that of isolating the O^+ 834 Å emission from much brighter airglow, most notably the H Lyman-α 1,216 Å emission. Although the utility of band pass filters for the EUV wavelength region of the spectrum has been reported in the literature (Seely and

Hunter, 1991; Chakrabarti et al., 1994; Zukic et al., 1992), in reality, the extrapolation from the soft x-ray region to the longer wavelengths has not been satisfactorily demonstrated. Work continues on this technology with encouraging results.

The instruments that would be necessary to make a substantial advancement in mapping O^+ 834 Å emission should consider the following parameters. It would need to have a good dynamic range (10^4 to 10^5 or better). The aurora, from a nightside vantage point, would represent the brightest signal which should be observed with reasonable spatial resolution (0.1° to 0.2°), comparable to the auroral imagers. A threshold of detection near 0.01 Rayleighs would be necessary to trace O^+ in the magnetosphere. For this, the angular resolution can be decreased by an order of magnitude to 1° to 2°, to make it comparable to ENA imager design goals.

References

Chakrabarti, S., Paresce, F., Bowyer, S., Chiu, Y.T., and Aikin, A. (1982): "Plasmaspheric Helium Ion Distribution From Satellite Observations of He 11 304 Å." Geophys. Res. Lett., vol. 9, p. 151.

Chakrabarti, S., Paresce, F., Bowyer, S., Kimble, R., and Kumar, S. (1983): "The Extreme Ultraviolet Day Airglow." J. Geophys. Res., vol. 88, p. 4898.

Chakrabarti, S., Kimble, R., and Bowyer, S. (1984): "Spectroscopy of the EUV (350-1400 Å) Nightglow." J. Geophys. Res., vol. 89, p. 5660.

Chakrabarti, S., Green, J.C., Chiu, Y.T., Robinson, R.M., Swenson, G.R., and Evans, D.S. (1986): "Imaging the Ionospheric Plasma Outflow in the Magnetosphere." Adv. Space Res., vol. 6, p. 215.

Chakrabarti, S., Edelstein, J., Keski-Kuha, R., and Threat, F. (1994): "Reflective Coating of 834 Å for Imaging O^+ Ions," Opt. Eng., vol. 53, p. 409.

Chiu, Y.T., Robinson, R.M., Swenson, G.R., Chakrabarti, S., and Evans, D.S. (19866): "Imaging the Outflow of Ionospheric Ions Into the Magnetosphere." Nature, vol. 322, p. 441.

Chiu, Y.T., Robinson, R.M., Collin, H.I., Chakrabarti, S., and Gladstone, G.R. (1990): "Magnetospheric and Exospheric Imaging in the Extreme Ultraviolet." Geophys. Res. Lett., vol. 17, p. 267.

Gladstone, R. (1992): "Simulated Images of the Plasmasphere." Proc. SPIE, vol. 1744, p. 171. "Instrum. for Mag. Imagery," Proc. SPIE, vol. 1744, edited by S. Chakrabarti, 1992. "Instrum. for Mag. Imagery II," Proc. SPIE, vol. 2008, edited by S. Chakrabarti, 1993.

Johnson, C.Y., Young, J.M., and Holmes, J.C. (1971): "Magnetoglow: A New Geophysical Resource." Science, vol. 171, p. 379.

Meier, R.R. (1990): "The Scattering Rate of Solar 834 Å Radiation by Magnetospheric O^+ and O^{++}." Geophys. Res. Lett., vol. 17, p. 1613.

Meier, R.R. (1991): "Ultraviolet Spectroscopy and Remote Sensing of the Upper Atmosphere." Space Sci. Rev., vol. 59, p. 1.

Murphy, D.L., and Chiu, Y.T. (1993): "Effects of Doppler Shifts and Source Perspectives on Extreme Ultraviolet Images of Ion Populations Moving in the Inner Magnetosphere." Geophys. Res. Lett., vol. 20, p. 2027.

Murphy, D., and Chiu, Y. (1993): "Geophysical Effects on Magnetospheric Images." Opt. Eng., vol. 32, p. 3147.

Seely, J.F., and Hunter, W.R. (1991): "Thin Film Interference Optics for Imaging the OII 834 Å Airglow." Appl. Opt., vol. 30, p. 2788.

Special Section on Mag. Imagery, Optical Eng., vol. 32, No. 12, edited by S. Chakrabarti, 1993.

Special Section on Mag. Imagery, Optical Eng., vol. 33, No. 2, edited by S. Chakrabarti, 1994.

Swift, D.W., Smith, R.W., and Akasofu, S.I. (1989): "Imaging the Earth's Magnetosphere." Planet. Space Sci., vol. 37, p. 379.

Williams, D.J., Roelof, E.C., and Mitchell, D.G. (1992): "Global Magnetospheric Imaging." Rev. Geophys., vol. 30, p. 183.

Young, J. M., Weller, C.S., Johnson, C.Y., and Holmes, J.C. (1971): "Rocket Observations of the Far UV Nightglow at Lyman Alpha and Shorter Wavelengths." J. Geophys. Res., vol. 76, p. 3720.

Zukie, M., Torr, D., Kim, J., and Torr, M. (1992): "Extreme Ultraviolet Filters for 58.4 and 83.4 nm." Proc. SPIE, vol. 1744, p. 178.

Radio Plasma Sounding

Remotely sensing and measuring distant plasma regions using emitted, reflected, and received radio waves is a technique that dates back to the study of the ionosphere from the ground by Breit and Tuve in 1926. The Alouette/International Satellites for Ionospheric Studies (ISIS) missions pioneered the use of space-borne swept-frequency sounders in order to obtain electron density profiles of the topside ionosphere. The technology of today's ground-based digital sounders (Reinisch, 1986) has progressed to the point that radio sounding can now be applied to magnetospheric plasmas (Green et al., 1993; Calvert et al., 1994) with very modest power requirements. Radio wave sounding of the magnetosphere uses the same fundamental principles as ionospheric sounding (for example, Hunsucker, 1991).

A radio plasma sounder (RPS) on the MI spacecraft would provide a major step forward in the ability to provide quantitative electron density profiles, from 0.1 to 10^5 cm^{-3}, simultaneously in several different directions and thereby provide important supplementary data for the core MI instruments. In addition, with an RPS, positions of critical plasma boundaries, such as the plasmapause and magnetopause, can be monitored on a time scale of a few minutes. Such simultaneous measurements have previously been impossible.

With its proposed orbit, MI will be well within the very low density region between the plasmapause and magnetopause for most of the time. Figure 7 schematically illustrates how RPS would work on MI. The dashed and dotted lines in figure 7 represent RPS echoes at two distinct frequencies. The echoes with the same frequency will reflect off the same density values (illustrated by the same contours in fig. 7). The three-axis antenna array is needed to determine the echo direction, while the RPS instrument measures the time delay (typically less than a second) of each echo giving the distance to the density structure.

The RPS instrument is ideal for studying the global structure and dynamics of magnetospheric plasmas such as the plasmasphere, a region of dense cold plasma of ionospheric origin surrounding the Earth, and its outer boundary, the plasmapause (Green et al., 1994). Many researchers have shown that the plasmasphere is very dynamic, with the plasmapause varying in distance between 2 and 7 R_E as magnetospheric conditions change from active to quiet. The RPS, unlike in situ measurements, can provide a sequence of nearly instantaneous plasmaspheric electron density profiles. Therefore, nearly the same region can be probed repeatedly within minutes, allowing the separation of spatial and temporal variations. Thus, the RPS instrument can provide, for the first time, observations of the formation of a plasmaspause boundary at a new location during substorms and of plasma trough refilling beyond a newly formed plasmapause. The distribution and movements of dense plasmas eroded from the main plasmasphere during substorms can be observed, thus permitting study of the mechanisms by which "detached" as opposed

to "connected" outlying cold plasma regions develop. Questions about the possible decoupling of the high-altitude and low-altitude convection regimes can be answered through correlative studies involving the RPS with other IMI instruments.

As illustrated in figure 7, the RPS will be an ideal instrument to investigate the time evolution of the density structures of the magnetopause boundary layers, to determine (1) the variability of plasma mantle density and thickness in response to the southward and westward components of the IMF and (2) the passage of kilometer size wave structures in the low-latitude boundary layer (i.e., Kelvin-Helmholtz waves). It could be readily determined from a sequence of sounder measurements whether the inner edge of the boundary layer moves only in phase with the magnetopause motion, or whether the thickness of the layer varies in time as the plasmas move downstream (Reiff et al., 1994).

The instrument would use two long dipole antennas in the satellite spin plane (500-m tip-to-tip length) and a short dipole along the spin axis (10-m tip-to-tip). Pulses with powers from a few milliwatts to a few watts will be transmitted from the long antennas. Current estimates are that the antennas weigh roughly 32 kg, with the instrument weighing roughly 3.25 kg, requiring about 11 W of power and generating a data rate of about 5 kbs/s with onboard processing and data compression.

References

Breit, G., and Tuve, M.A. (1926): "A Test for the Existence of the Conducting Layer." Phys. Rev., vol. 28, p. 554–575.

Calvert, W., Benson, R.F., Carpenter, D.L., Fung, S.F., Gallagher, D., Green, J.L., Reiff, P.H., Reinisch, B.W., Smith, M., and Taylor, W.W.L. (1994): "The Feasibility of Radio Sounding of the Magnetosphere." Submitted to Radio Sci., 1994.

Green, J.L., and Fung, S.F. (1994): "Radio Sounding of the Magnetosphere From a Lunar-Based VLF Array." Adv. Space Res., vol. 14, No. 6, pp. 217–221.

Green, J.L., Benson, R.F., Calvert, W., Fung, S.F., Reiff, P.H., Reinisch, B.W., and Taylor, W.W.L. (1993): "A Study of Radio Plasma Imaging for the Proposed IMI Mission." NSSDC Technical Publication, February 1993.

Hunsucker, R.D. (1991): "Radio Techniques for Probing the Terrestrial Ionosphere." Phys. Chem. Space. vol. 22, Springer Verlage, Berlin.

Reiff, P.H., Green, J.L., Benson, R.F., Carpenter, D.L., Calvert, W., Fung, S.F., Gallagher, D., Reinisch, B.W., Smith, M.F., and Taylor, W.W.L. (1994): "Radio Imaging of the Magnetosphere." Feature article in EOS, vol. 75, pp. 129, 133, and 134.

Reinisch, B.W. (1986): "New Techniques in Ground-Based Ionospheric Sounding and Studies, Radio Sci., vol. 21, No. 3, pp. 331–341.

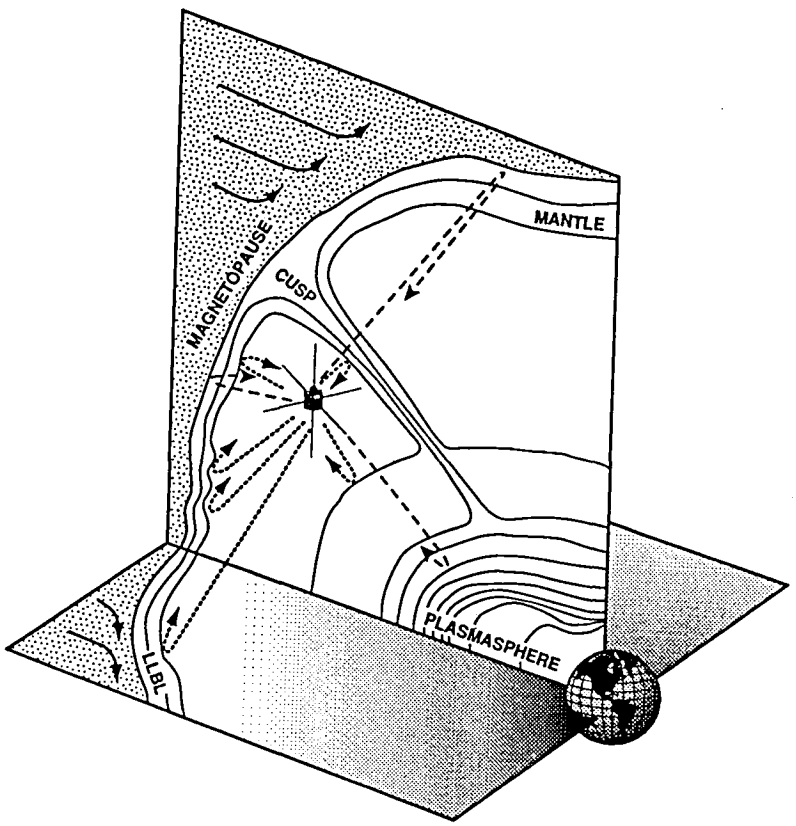

Figure 7. Radio wave sounding of magnetospheric plasma structures.

Electron Densities from Global Positioning System Signals, Global Positioning System (GPS) Receiver on MI for the Measurement of Magnetospheic Ionization Content

A GPS receiver on the MI satellite could provide total electron content (TEC) along the line of sight between MI and any one of up to 10 GPS satellites at any given time. Each GPS satellite transmits two precision L-band signals along a cone sufficient to cover near-Earth receiver operations at up to 1 R_E in altitude. In addition, the GPS cross-ranging system transmits two precision VHF signals centered at 50° below the GPS horizon, covering a conic annulus above 4 R_E.

In positioning operations, these signals are picked up by appropriate receivers that infer positions from time delays in the navigation message. Since these signals have to pass through the ionosphere and/or the plasmasphere, refraction plasma delays would be introduced into the signals. To compensate for the plasma delays, two frequencies are transmitted with each type of signal. Since plasma delays are frequency-dispersive, the measurements of delays at two frequencies (a pair at L-band and a pair at VHF) allow the receivers to correct for the integrated delay introduced by the ionospheric and/or plasmaspheric total electron content. In positioning operations, the differential time delay information is used as a correction but is not kept. With modified GPS receivers (developed for several test missions in the 1995 to 2000 time frame) on MI, however, the ionospheric/plasmaspheric correction could be obtained and the signal recorded. This technique has been widely used to make ionospheric total electron content measurements using the GPS receivers on the ground and is manifested for a number of NASA, ESA, and DOD space missions starting in 1995.

As GPS satellites orbit at 4 R_E altitude, they are suitably located for making high-altitude TEC measurements for regions above the ionosphere. By carrying special L-band and VHF GPS receivers, the MI spacecraft could make line-of-sight TEC measurements between MI and GPS satellites either above or at the other side of the inner magnetosphere. Simulation studies have shown that such TEC's can be mapped within an 8 R_E sphere. These measurements would reflect the true integrated total ion electron content along a variety of plasmaspheric lines of sight and so would serve as a direct measurement supporting the He^+ 304 observations. (The EUV measurements of He^+ 304 represents only the He^+ component of the plasmasphere.) He^+ 304 is generated by resonance scattering and so the observed intensity also depends on the strength of the solar emission at this wavelength. Moreover, the proposed MI orbit would provide optimal coverage of the outer plasmasphere via TEC measurement from GPS cross ranging (VHF) signals. The GPS technique provides a direct measurement independently of other factors.

In summary, GPS line-of-sight TEC measurements would provide an excellent data set on plasmaspheric structure and dynamics. It would also serve to support the He^+ 304 measurements by providing an independent measure of the total density (via deconvolution of TEC measurements) and would thus indicate the density ratios between He^+ and other ions (e. g., H^+).

RELATIONSHIP OF MAGNETOSPHERIC IMAGING TO IN SITU AND GROUND-BASED SCIENCE

With the MI space scientists will have "support" imagery of magnetospheric structures available for the first time. The technique of combining imagery with in situ observations will clarify and enhance the scientific interpretation of both the imagery and the point-wise observations.

It should be possible to establish by this method what volumes of the magnetosphere change in what characteristic and by how much in response to major events such as substorms. The importance of imagery to clarify the interpretation of detailed planetary and solar features has been widely appreciated. The availability of information on the shapes, positions, and intensities of magnetospheric features will benefit diverse research areas. If missions are conducted concurrently, MI could support ionospheric, thermospheric, and interplanetary flight investigations. While the SDT concludes that the MI science objectives can be met using the observations described here as "core," there are many and substantial benefits to be gained from also acquiring in situ observations in the MI-observed structures. Establishing the relationship between familiar in situ local signatures and global magnetospheric structures has enormous value. An illustration of this type of relationship occurs in meteorology. Consider the benefit to the interpretation of global scale tropospheric weather features observed by satellite of having point-wise pressure, temperature, and wind observations from radiosondes and the ground. In the case of MI, since the emissions are from optically thin regions, in situ observations taken throughout the region will be synergistic with the images.

MAGNETOSPHERE IMAGER (MI) SOLAR TERRESTRIAL PROBE CLASS MISSION PRELIMINARY DESIGN STUDY

MISSION DEFINITION

The MI was originally conceived to be a part of the Space Physics Division's intermediate class of missions with a cost ceiling of $300M. The engineering studies performed at MSFC indicated that a spinning spacecraft with a despun platform, similar to General Electric's (now Martin Marietta) POLAR and Hughes' HS-376 spacecraft, launched aboard a Delta, could easily accommodate the strawman science instruments defined by the MI SDT. A summary of the intermediate-class MI mission spacecraft and instrument complement is listed in table 1.

Table 1. Options for the MI mission.

	Intermediate Class Mission	Solar Terrestrial Probe Mission
Cost Ceiling ($)	300M	150M
Launch Vehicle	Delta II	Conestoga, Taurus, or Lockheed launch vehicle (LLV)
Orbital Parameters	4,800 by 44,600 km (7 R_E) 90°	4,800 by 44,600 km (7 R_E) 90°
Instruments	Seven (four on spinning spacecraft; three on despun platform)	Three "core" (one is a consolidation of three from the original list) plus up to three "mission enhancing"
Total Spacecraft Mass (kg) (wet; including 30-percent contingency)	1,000 (HS-376) 1,300 (POLAR)	413

In the summer of 1993, the MI SDT and MSFC engineering team were directed by the Space Physics Division to redefine the MI mission to fit within a new class of missions, the Solar Terrestrial Probe (STP). STP missions must cost no more than $150M (excluding launch cost) and be accommodated on launch vehicles smaller than a Delta. The MI SDT met in November 1993 and developed a new strawman instrument complement suitable for a smaller spacecraft but still capable of meeting the core science objectives necessary for magnetospheric imaging. This section summarizes the preliminary results of the MI STP design study.

SCIENCE INSTRUMENT COMPLEMENT

The MI SDT developed the initial strawman instrument complement for the mission. It consisted of seven instruments with a total mass of 187 kg, requiring 190 W of power. Four instruments operated in a scanning mode and three instruments operated in a staring mode; therefore, requiring a spinning spacecraft with a despun platform. The STP mission guidelines necessitated the development of a new strawman instrument list by the SDT. This list includes three core instruments and three enhancing instruments as described in table 2. The concepts discussed in this report only accommodate the three core instruments. The addition of enhancing instruments will be considered in future studies. The instruments' technical parameters were also provided by the SDT. Other sources have indicated that a reduction in instrument electronics by 30 percent in volume, mass, and power is possible. This reduction was presented to the SDT and was considered reasonable, but not preferred.

Table 2. MI STP strawman instrument list.

Instrument Name	Field-of-View (FOV)	Dimensions (W×D×H) m	Mass (kg)	Power (W)	Data (kb/s)	Point Acc. (degree)
CORE						
Hot Plasma Imager (H)	4π str	0.51×0.35×0.51	14.0	4.0	12	5.0
Hot Plasma Imager (L)	4π str	0.30×0.30×0.25	7.0	7.0	6	
Electronics		0.30×0.30×0.30	8.0	12.0		
Plasmasphere Imager (He+304)	135°×180°	0.48×0.16×0.20	7.2	4.5	7	0.5
Electronics		0.23×0.18×0.20	11.8	16.5		
FUV Imager and Electronics	40°×360°	0.70×0.80×0.30	30.0	25.0	15	
Total			78.0	69.0	40	1.0
ENHANCING						
Plasmasphere Imager (O+834)	135°×180°	0.48×0.16×0.20	7.2	4.5	7	0.5
Electronics		0.23×0.18×0.20	11.8	16.5		
Electron Precipitation Imager	3°×3°	0.20×0.20×0.60	24.5	11.0	2	0.3
Electronics		0.25×0.18×0.18	3.0	9.0		
Radio Sounder (four units)		0.22×0.12×0.12	35.2	10.8	6	
Spin Axis Antenna (two units)		0.50×0.20×0.18				
Electronics		0.20×0.18×0.15				

Two of the core instruments are from the original MI instrument list but the third, the Far Ultraviolet (FUV) Imager, is a combination of three ultraviolet imagers from the original instrument complement: two staring and one scanning. All three core instruments operate in the scanning mode, eliminating the requirement for a despun platform. The total core instrument mass is 78 kg and the power requirement is 69 W. The Electron Precipitation Imager must operate in a staring mode and would require the addition of a despun platform, driving up the cost and complexity of the mission. The other two enhancing instruments operate in a scanning mode, thus making their potential inclusion to the current MI STP mission somewhat less difficult.

MISSION ANALYSIS

The MI mission orbit has a perigee altitude of 4,800 km, and an apogee altitude of 44,600 km (7 R_E). The apogee of 7 R_E was a requirement specified by the SDT, and the perigee altitude of 4,800 km was driven by the performance capability of the POLAR spacecraft propulsion system, the intermediate class mission spacecraft mass, and the Delta II launch vehicle performance capability. Other concerns driving the orbit selection included avoiding monatomic oxygen in the upper atmosphere at the 1,000- to 1,500-km altitudes and high plasma densities at altitudes less than 4,800 km. Because of these environmental constraints and to maintain instrument viewing perspective, this orbit is considered nominal for the solar terrestrial probe mission.

The achievable perigee is dependent upon the amount of propellant that can be loaded onto the spacecraft, the spacecraft mass, and the launch vehicle capability. The IMI SDT asked that a trade study be performed to determine the available payload mass as a function of perigee altitude for the current STP option. The results, presented in figure 8, can be summarized by stating that for every 100 km the perigee is reduced, 1 kg of additional mass (science instrument or spacecraft) can be placed into the desired orbit. Any spacecraft subsystem mass changes directly affect the science instrument mass that can be accommodated.

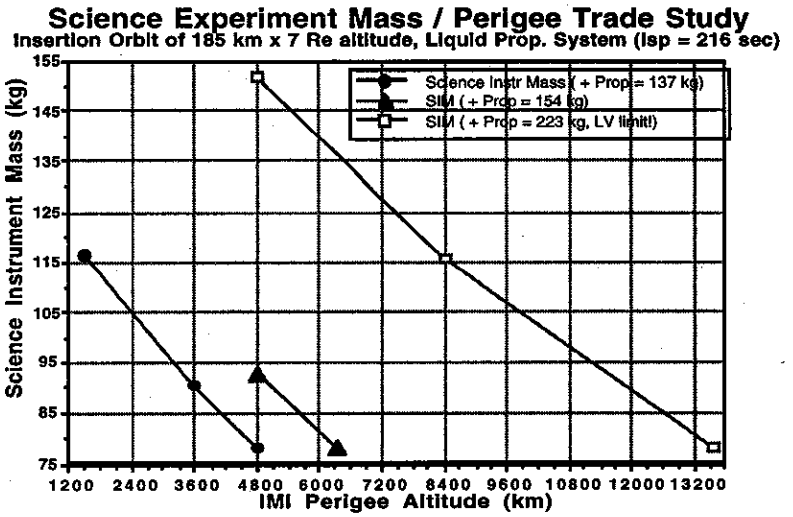

Figure 8. Experiment mass/perigee trade study.

LAUNCH VEHICLES

Three launch vehicles, the Taurus 120 XL/S, Conestoga 3632, and Lockheed LLV3, were considered for the STP option. Performance estimates for the insertion orbit of 185 km by 7 R_E were generated by the respective vehicle manufacturers and the capability of each vehicle is graphically represented in figure 9. The values for the 185-km perigee insertion assume that the spacecraft's propulsion system will be used to achieve the final 4,800-km by 7-R_E orbit.

The configuration description and capabilities of the vehicles that were under consideration are discussed briefly in the following paragraphs.

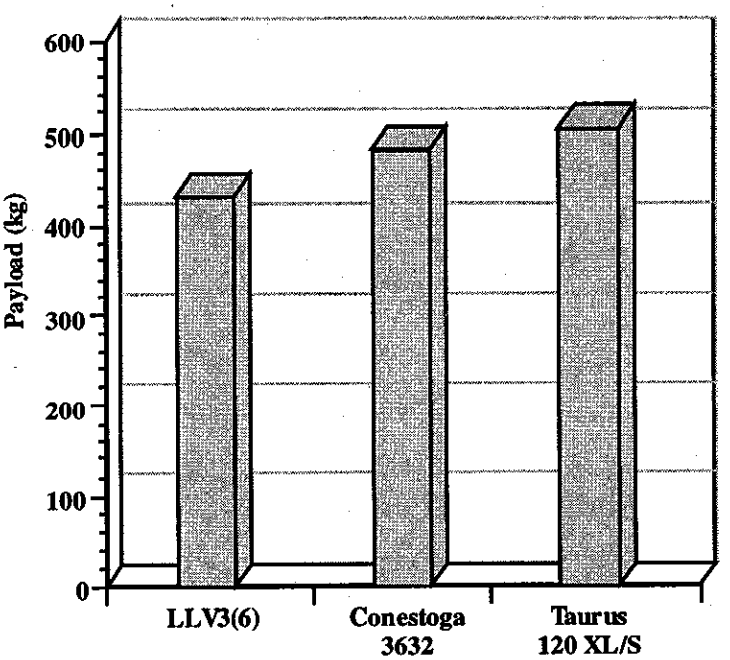

Figure 9. Launch vehicle capabilities.

Taurus 120 XL/S

The Taurus 120 XL/S is being developed by Orbital Sciences Corporation (OSC) and is the smallest launch vehicle that is capable of completing the mission objectives. The first vehicle in the Taurus line was launched successfully in March of 1994. The initial launch of the Taurus XL vehicle should occur soon, while the 120 XL/S is an enhanced model that is not projected to be operational until 1995. The Taurus is composed of Pegasus upper stages lifted by a Thiokol Castor 120 solid motor. In addition, it utilizes two GEM's as strap-on boosters. Based on analysis by OSC, the Taurus will place 500 kg into the 185-km by 7-R_E orbit. The Taurus dynamic payload envelope is 1.4 m, but the IMI spacecraft power and surface area requirements necessitate the consideration of other launch vehicles with larger dynamic payload envelopes.

Conestoga 3632

The Conestoga family of launch vehicles is currently under development by EER Systems, Inc. The scheduled launch of the first all-solid Conestoga vehicle is mid-1994. Commonality of the solid motors is the basis of the Conestoga family. For this mission, the five-stage Conestoga 3632 is necessary. The first three stages are comprised of the core Castor IVB XL and the surrounding two Castor IVA XL and four Castor IVB XL strap-on motors. The fourth and fifth stages are an Orion 50 XL and a Star 48V, respectively.

EER Systems estimated the performance of the Conestoga 3632 to insert a payload mass of 481 kg into the 185-km by 7-R_E orbit. This requires the spacecraft to have an onboard propulsion system to achieve the final desired orbit placement. The total payload mass includes not only the separated spacecraft, but also any special attachment structures which may be required. Although the boost capability of this vehicle is less than the Taurus XL/S, the larger payload dynamic envelope of 1.6 m makes it an attractive option.

LLV3(6)

The LLV is a new series of small launch vehicles, with the first flight scheduled in 1994. The LLV3(6) is the smallest member of this family to meet the requirements of the IMI mission. This vehicle, like the Conestoga, is composed of solid motors. The first two stages require a Castor 120, and the third stage is an Orbus 21D. In addition to these motors, there are six first-stage strap-on Castor IVA motors. An Orbit Adjust Module (OAM), located above the Orbus 21D, is attached to the payload. The OAM provides various control functions during flight and can be used for additional maneuvers, such as transfer burns.

With this configuration, Lockheed estimates that 428 kg can be placed into the 185-km by 7-R_E orbit with a payload dynamic envelope of almost 2 m. With additional hydrazine propellant in the OAM, the LLV3(6) can place the spacecraft into the 4,800-km perigee orbit. However, the performance is reduced to 288 kg.

MI STP Baseline Vehicle

The launch vehicle chosen for the MI STP mission, based on performance estimates and fairing size, is the Conestoga 3632 presented in figure 10. Included in figure 10 is a closeup view of the 4.9-m payload fairing.

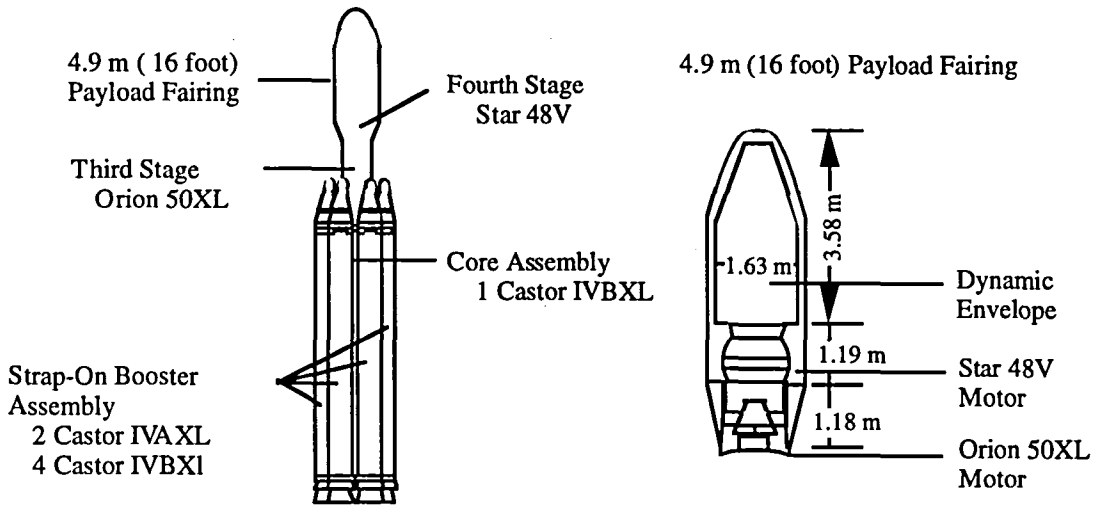

Figure 10. Conestoga 3632 launch vehicle.

CONFIGURATIONS

The baseline configuration for the MI spacecraft presented in figure 11 is sized to fit a medium launch vehicle, such as the Conestoga 3632 or Lockheed (LLV3) launch vehicle. The instrument complement includes the three core instruments: the Hot Plasma Imager, the Plasmasphere Imager (He+304), and the FUV Imager.

The spacecraft diameter of 1.5 m was chosen as a compromise between launch vehicle payload capacity, power system surface area requirements, and spacecraft stability requirements. Minimizing the spacecraft size reduces the mass. Maximizing diameter and minimizing spin axis length improves spin stability. The spacecraft length of 1.3 m provides sufficient side wall surface area for solar cells, radiators, antennas, and science instrument view ports. The length is also dictated by the spacecraft subsystems and scientific instrument volumes.

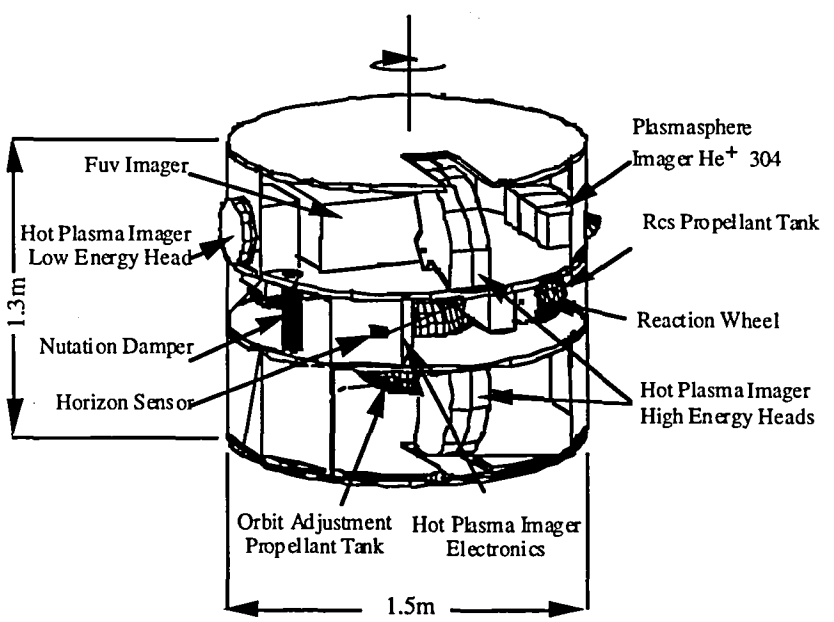

Figure 11. MI STP preliminary design baseline configuration.

The spacecraft subsystems and science instruments are arranged within the spacecraft to optimize the mass moments of inertia. Placement of the science instruments is restricted by their FOV requirements. The spacecraft subsystems are positioned to account for balancing and compatibility with adjacent components. The addition of any mission-enhancing instruments will necessitate rearrangement of the internal components.

STRUCTURES

The baseline structural design of the spacecraft, shown in figure 12, consists of three aluminum honeycomb plates supported by a side wall and longerons constructed from either aluminum or graphite composite. Modifications to the spacecraft to accommodate the radiator band will result in changes to the plates, which are no longer required to reject heat. These panels may now be fabricated from a graphite composite, although the material selection will be a trade of cost and mass. Construction method, materials selection, and configuration changes will result in a shifting of the structural masses, but no significant mass change is expected. Structural design and analysis will continue to define the configuration of the spacecraft.

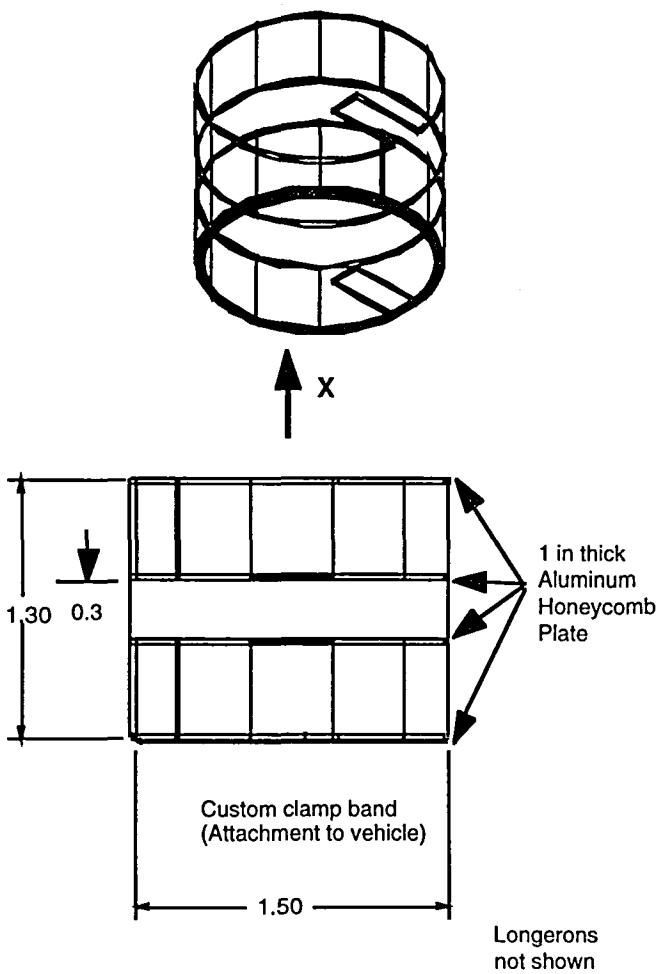

Figure 12. Spacecraft structure.

ELECTRICAL POWER SYSTEM

Electrical power load requirements for the spacecraft are estimated to be 182.2 W. The total power requirements represent 69 W for the three-instrument payload suite, with the remaining power designated for other subsystems, housekeeping, and contingency. The power subsystem requirements, components, and masses are listed in table 3.

The polar orbiting spacecraft is spin-stabilized with body-mounted solar cells on the cylindrical section and both ends. Total active solar array surface area is estimated to be 7.58 m^2 with a maximum effective illumination area of 2.1 m^2, as shown in figure 13.

Platform orbit orientation of the spin axis is normal to the orbit plane. The results of this orbital profile is a worst-case angle of a ±66.5° between the Sun vector and the orbital plane (beta angle). At these angles, the solar array power output is 363 W. The worst-case beta angle of 0° will give a power output of 252 W. This will result in a power margin of 70 W between the solar array output and the total load demand at end-of-life (EOL) shown in figure 14.

Table 3. Electrical power subsystem summary.

Instrumentation Suite, Core (Full Electronics Power)	
– Hot Plasma Imager (H)	4.0 W
– Hot Plasma Imager (L)	7.0 W
– Electronics	12.0 W
– Plasmasphere Imager(He+304)	4.5 W
– Electronics	16.5 W
– FUV Imager and Electronics	25.0 W
Subtotal:	69.0 W (avg.)
Subsystem Electrical Power Requirements	
– Communications and Data Handling	32.0 W
– Transponder (@ 7-percent duty cycle)	
– Guidance, Navigation, and Control	42.0 W
– Thermal (@ 70-percent duty cycle)	14.0 W
Subtotal:	88.0 W (avg.)
Total Electrical Power Load	
– Instrument Suite	69.0 W
– Subsystems	88.0 W
– Contingency (15 percent)	25.2 W
Total:	182.2 W (avg.)
Surface Area Available (Assumed):	
– Cylindrical Surface: 72 percent	4.40 m^2
– End Surfaces (Two): 90 percent	3.18 m^2
EPS Mass:	
– Solar Arrays	7.74 kg
– Electronics	7.26 kg
– Battery	9.52 kg
– Cabling/Harnesses	20.11 kg
Total:	44.63 kg

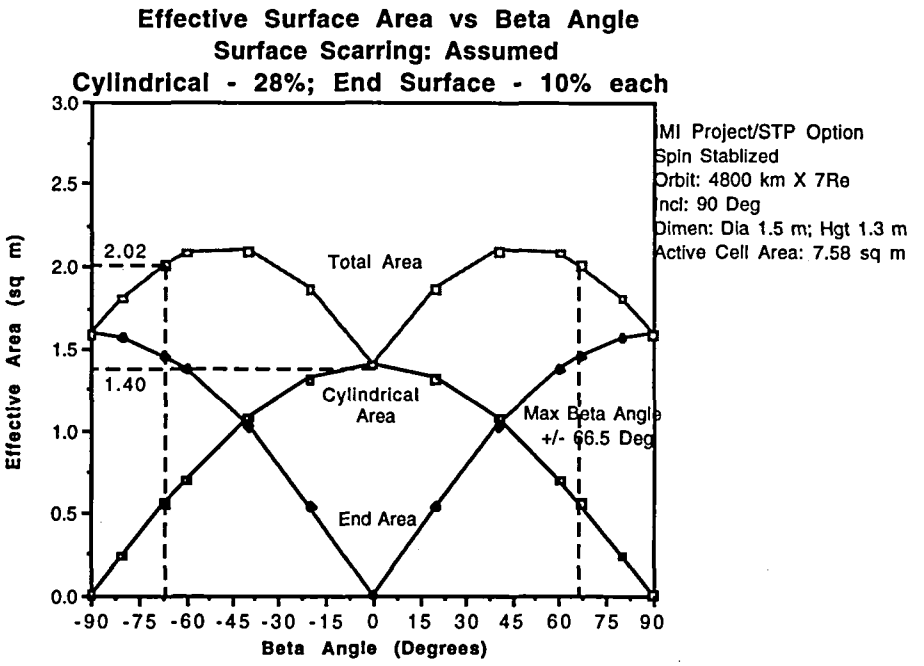

Figure 13. Effective area versus beta angle.

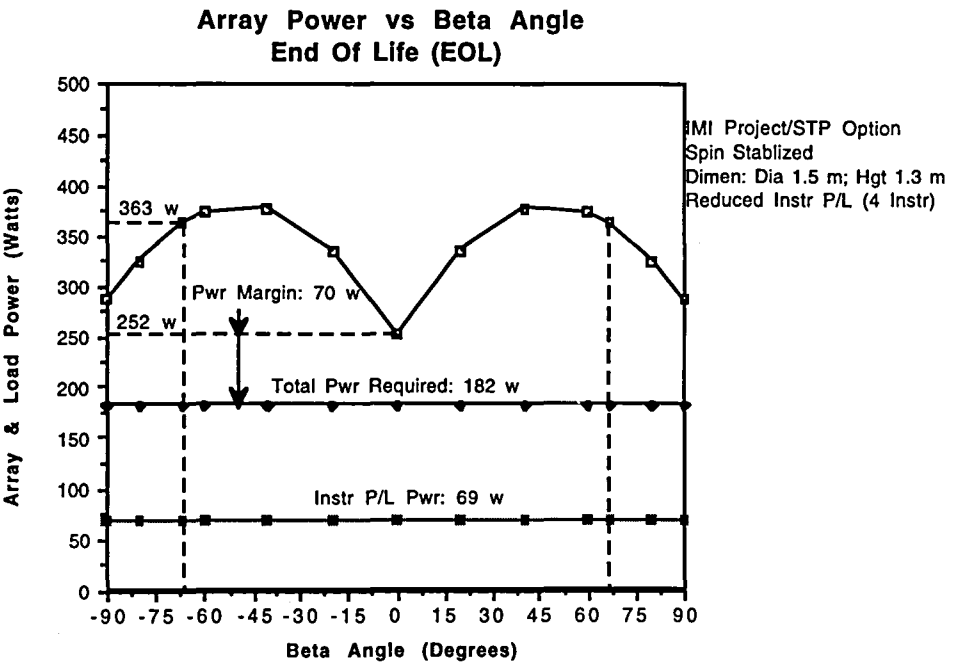

Figure 14. Solar array load power versus beta angle.

Power calculations are based upon an 18.5-percent efficient gallium arsenide (Ga-As) cell. A trade study was performed on several types of Ga-As cells:

- 2- by 4-cm, 3.5-mils thick, 18.5-percent efficient (baseline)
- 4- by 4-cm, 5.5-mils thick, 18.6-percent efficient
- 5.5- by 6.5-cm, 5.5-mils thick, 18.1-percent efficient.

The 2- by 4-cm cell was chosen as the baseline solar cell for the mission. Two batteries were considered: a new small satellite nickel hydrogen (Ni-H_2) cell design and a nickel metal hydride (Ni-MH) battery. The Ni-H_2 cell design was chosen for the baseline.

THERMAL CONTROL SYSTEM

The possible addition of the radio sounder, with the attendant requirement to not perform a 180° spacecraft maneuver every 6 months, presents some solar incident radiation problems for the thermal control system. Without flipping the spacecraft, the surfaces used for thermal radiators will be exposed to solar heating for extended periods, thereby degrading the performance of the radiators. Furthermore, there is no position on the spacecraft that radiator panels could be located that would not at some time during the mission be exposed to the Sun. The 180° flip provides an ideal heat sink to deep space for the spacecraft systems thermal loads and the FUV detector which needs to be maintained at about –100 °C.

Two options, shown in figures 15 and 16, were considered for thermal control of the spacecraft in the absence of an orbital "flip" maneuver: (1) locating the radiator surfaces on the ends of the spacecraft and (2) locating the radiator on the cylindrical body of the spacecraft. The thermal control system design was forced to consider impacts on the electrical power system design because both require part of the scarce surface area of the spacecraft body. Option 1 would require that the radiator and solar arrays share the ends of the spacecraft. A requirement of the electrical power system only allows the thermal radiators 30 percent of the spacecraft ends which is about 0.5 m^2 for each. Option 2 requires that the solar arrays and the thermal radiators share the cylindrical portion of the spacecraft, leaving the ends free for solar arrays. The radiating surfaces would need to have optical properties similar to those of the shuttle orbiter radiators, which have a low absorptivity ($\alpha = 0.09$) and a high emissivity ($\varepsilon = 0.81$). This optical surface reflector (OSR) would limit the solar radiation absorbed by the radiator while still allowing the surface to radiate effectively.

Steady-state thermal analyses were performed to evaluate the performance of the two concepts. The end-mounted radiators were modeled in their worst-case condition, where one end of the spacecraft is facing the Sun and the other is opposite the Sun. The analysis of this concept showed that only about 168 W of heat could be rejected at 273 K. Using 0.6 m^2 or 34 percent of the end surface area, 193 W could be rejected, which is about 10 W more than the 182 W required. Results of the analysis of the radiator mounted on the cylindrical portion of the spacecraft, shown in figure 17, indicate that a band approximately 0.2-m wide about the circumference of the body would reject the 193 W in the worst-case condition when the spacecraft cylinder is normal to the solar vector. Therefore, the baseline design is to locate the thermal radiator on the cylindrical portion of the spacecraft.

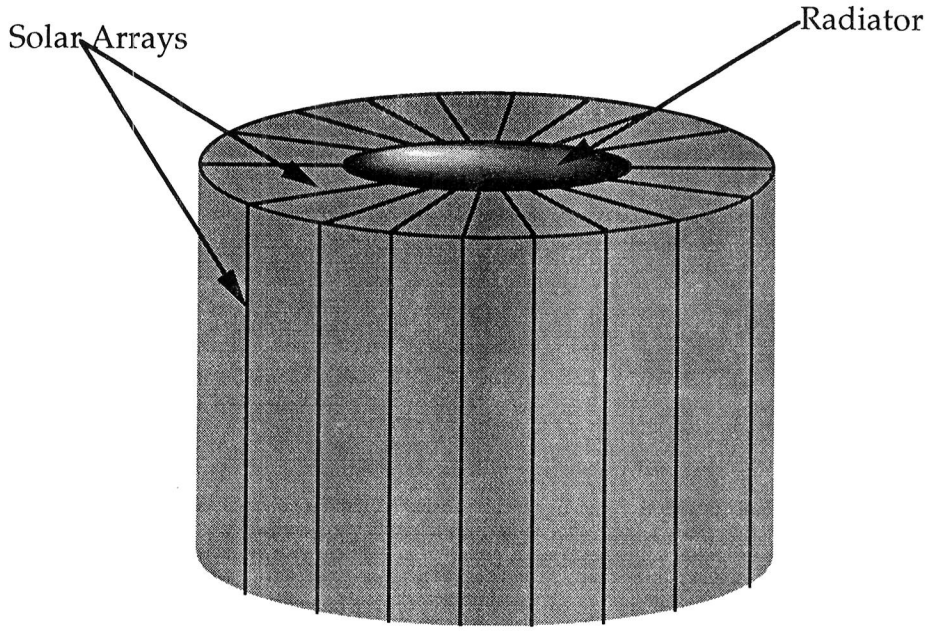

Figure 15. MI with radiators on spacecraft ends.

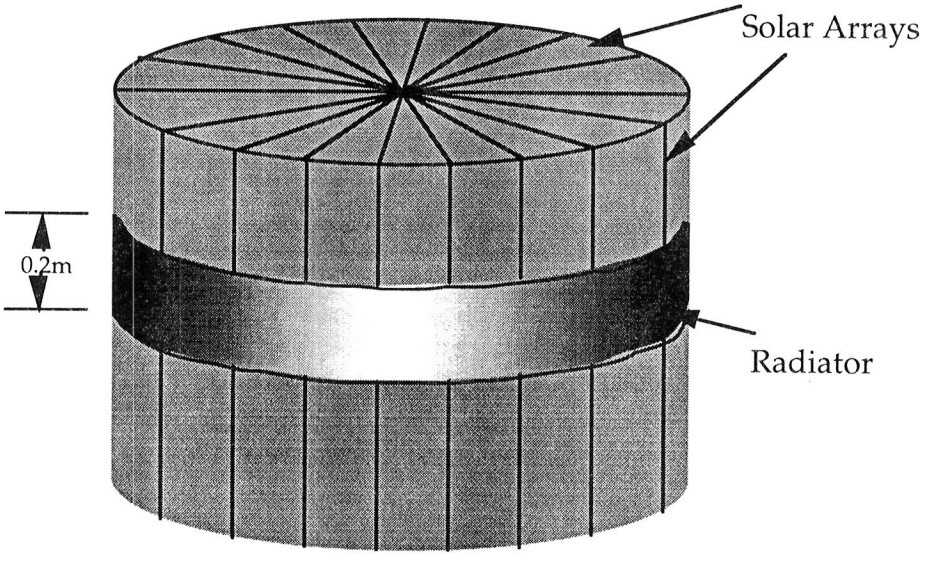

Figure 16. MI with radiator on cylindrical section of spacecraft.

ATTITUDE CONTROL SYSTEM

The spacecraft attitude control system should provide a stable spinning platform that meets the science instrument pointing requirements of 0.5° for knowledge, accuracy, and stability over a 1-min period. The spacecraft system should also provide guidance, navigation, and control during orbit transfer from separation of the launch vehicle upper stage to the orbit perigee. Requirements during orbit transfer include a full inertial reference system with sensors and algorithms for orbit and attitude determinations

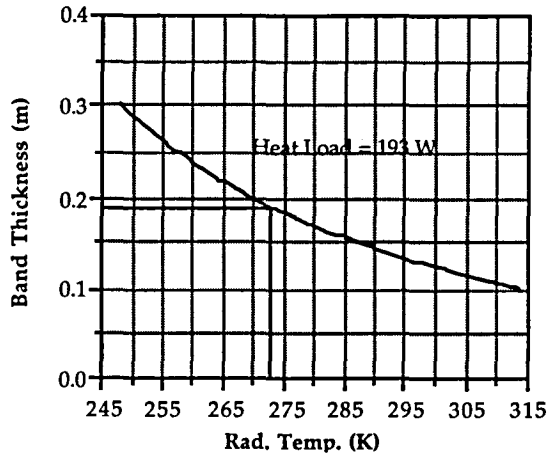

Figure 17. Radiator band size versus radiator temperature.

and a complement of reaction control system (RCS) thrusters to maintain vehicle attitude during orbit transfer. After the spacecraft attains orbit perigee, the RCS thrusters will align the spacecraft spin axis along the orbit normal, remove attitude errors, and then spin the spacecraft to the required 10 rpm. Attitude sensors include rate gyros, fine and coarse Sun sensors, and horizon sensors. A spin-axis damper located at the spacecraft perimeter will provide passive nutation damping. The RCS could augment this nutation damping and provide spin axis control, if needed.

To avoid orbit perturbations due to RCS forces, six pairs of thrusters apply pure couples on the spacecraft and employ simpler control algorithms than those needed for single thrusters. A representation of the spacecraft attitude control system is shown in figure 18. The four pairs of pitch-thrusters will be replaced by two pairs.

The directional stability of the spacecraft and damper system was assessed for the 1.3- by 1.5-m configuration. The equations of motion in the body-fixed reference frame $\{x_r, y_r, z_r\}$ of figure 19 are:

$$\dot{\boldsymbol{p}} = -\boldsymbol{\omega}\times\boldsymbol{p}+\boldsymbol{f}\,,$$

$$\dot{\boldsymbol{h}} = -\boldsymbol{\omega}\times\boldsymbol{h}-\boldsymbol{v}\times\boldsymbol{p}+\boldsymbol{g}\,, \tag{1}$$

$$\dot{p}_d = m_d\omega^T\boldsymbol{j}\times(\boldsymbol{v}-\boldsymbol{r}_d\times\boldsymbol{\omega})-c_d\dot{\xi}-k_d\xi\,,$$

where $\boldsymbol{p}$ is the system linear momentum, $\boldsymbol{h}$ is the system angular momentum, $\boldsymbol{v}$ the body velocity, $\boldsymbol{\omega}$ the angular velocity, and $\boldsymbol{r}_d$ is the location of the damper with respect to the body center-of-mass, where $\boldsymbol{r}_d = b\boldsymbol{i} + \xi\boldsymbol{j}$. The sum of external disturbance forces and thruster control forces is $\boldsymbol{f}$, and the sum of external disturbance torques and RCS torques is $\boldsymbol{g}$. The attitude equations are linearized for small perturbations, using small attitude angles α_1, α_2, α_3. Perturbations about the spin axis are not stable and will not be influenced by the axial damper, so the states are chosen to be $\{\alpha_1, \alpha_3, \xi\}$. The linear system is stable if the system eigenvalues are in the left half plane. Necessary and sufficient conditions for stability can be determined by the following Routh-Hurwitz criteria.

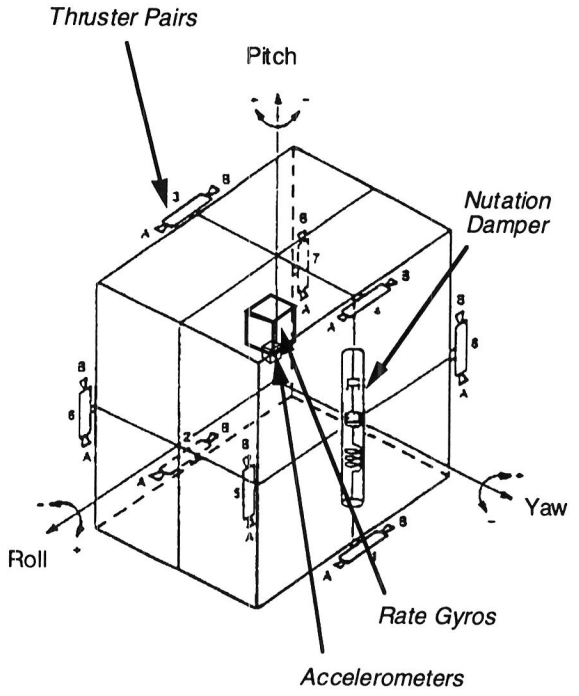

Attitude Sensors:
2 coarse Sun sensors
2 fine Sun sensors
2 high resolution horizon sensors

Figure 18. Attitude control system components.

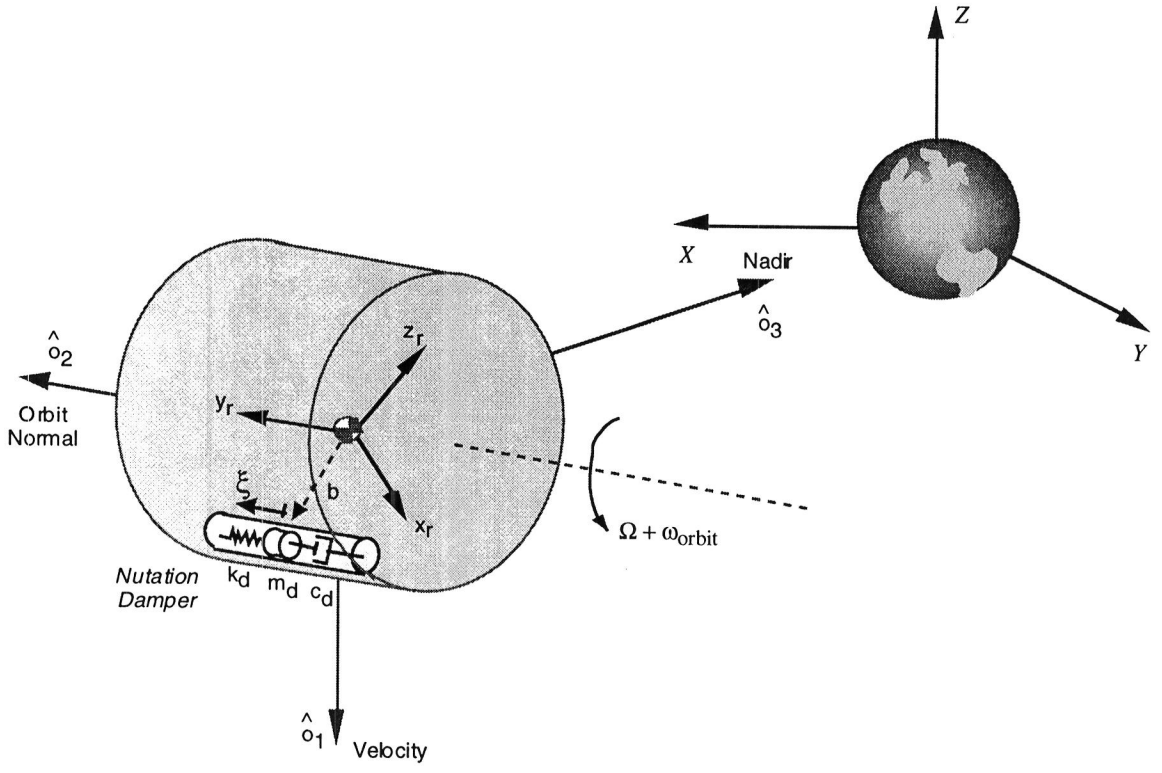

Figure 19. Coordinate frames.

$$k_1 = (I_2 - I_3)/I_1 > 0$$

$$k_{3d} = k_3 - v^2 \frac{m_d b^2 / I_3}{k_d / m_d} > 0 \qquad (2)$$

where

$k_3 = (I_2 - I_1)/I_3$.

The principal moments of inertia used for this analysis are I_1 = 101.2 kg m^2, I_2 = 114.5 kg m^2, and I_3 = 94.6 kg m^2. The corresponding spacecraft mass used is 320.5 kg which is an early mass estimate including a 30-percent contingency. The damper mass is 1 kg, and the spin rate v is 10 rpm. The damper properties can be chosen by selecting the damper eigenvalues to match those of the system without the damper, or by examining a root locus of the system eigenvalues for a range of damper parameters. The nutation eigenvalues in the root locus range from damping factors of $\zeta = 0.4$ for k_d of 0.08, to $\zeta = 0.0013$ for k_d of 1.1, with corresponding settling times of approximately 1 min to 4 h. Both techniques yield a directionally stable system using the criteria from equations (2). The damper characteristics will be selected to meet the mission requirements determined by the science instruments.

An estimate of disturbance torques for MI is shown in figures 20 to 23. The orbit is 4,800-km altitude by 7 R_E, on March 21, 2001, using a 2σ Jacchia density model. Magnitudes of the solar radiation torque, gravity gradient torque, and aerodynamic torque are plotted in figures 20, 21, and 22, respectively. Figure 23 shows the sum of these torques about the spacecraft x, y, and z axes. RCS propellant usage to manage these torques is estimated at 1 kg over the 2-yr lifetime. An additional 1 kg of propellant is needed for initial reorientation and spin-up after orbit acquisition, and 5 kg of propellant is estimated for RCS control during the orbit insertion.

The attitude control system equipment list includes one nutation damper, two coarse and two fine Sun sensors, two high-resolution horizon sensors, three rate gyros, two single-axis accelerometers, control electronics, and cabling. The total system mass estimate is 22 kg, with a total power estimate of 42 W.

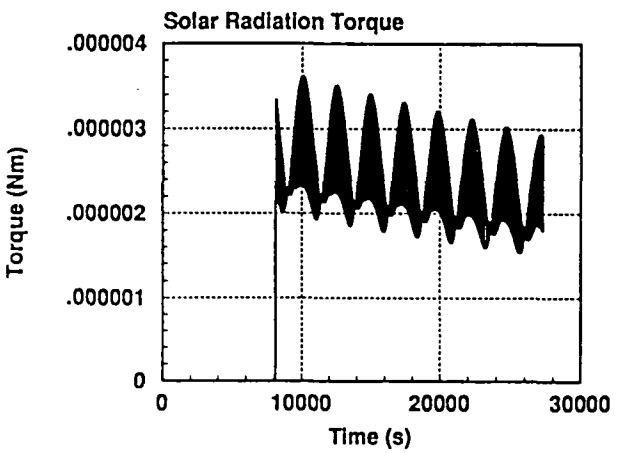

Figure 20. Solar radiation torque.

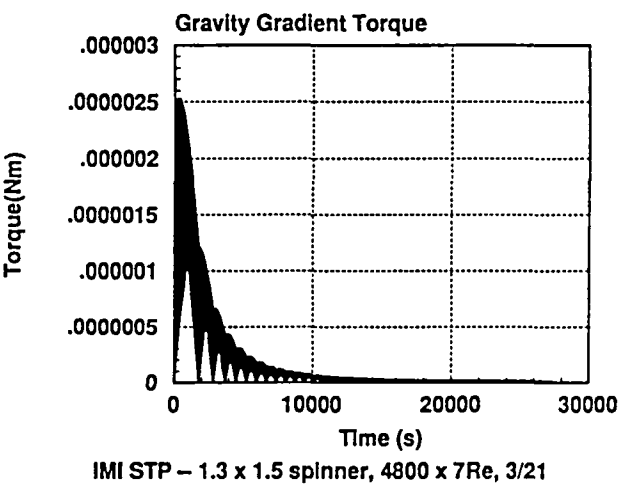

Figure 21. Gravity gradient torque.

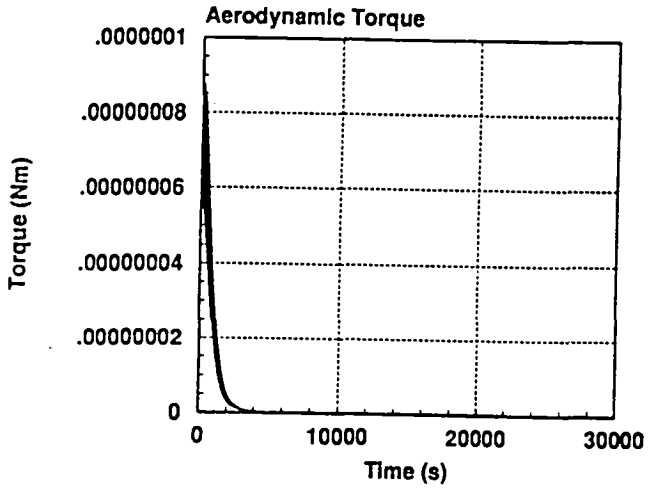

Figure 22. Aerodynamic torque.

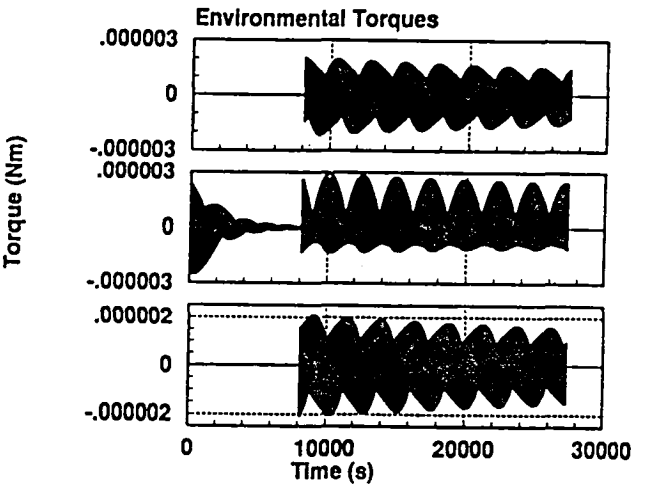

Figure 23. Environmental torques.

PROPULSION

Two options were considered for the spacecraft propulsion system. The first baselined an off-loaded Star 17 solid propellant motor for the orbital reboost with a blowdown monopropellant hydrazine RCS. The mass summary for this option indicates that the total payload mass exceeds the launch vehicle capability: structural accommodation would require a thrust structure, a mission specific payload attachment fixture, and a minimum of two separation systems. An all-liquid blowdown monopropellant hydrazine propulsion subsystem was, therefore, selected following a trade study which indicated that the overall payload weight was reduced due to elimination of the motor structural accommodations required.

A trade of the options for number of tanks required, placement of the tanks, and the systems operation were all taken into account in the design of the propulsion system. The design consists of two systems: RCS and orbit adjust. The orbit adjust is accommodated by using a single 55.73-cm (21.94-in) diameter tank located along the vehicle centerline with two nominal 66.75-N (15-lbf) thrusters on the spacecraft aft end. A single string isolation system is assumed with all hardware being "off-the-shelf."

The RCS is a similar design based on the same philosophy. Two 23.29-cm (9.17-in) diameter tanks are required in order to keep the spinning spacecraft balanced as the propellant is depleted. The tanks are located in the plane of the vehicle center-of-mass. Bladders are also required as the RCS provides attitude control during orbit transfer. The tanks are purposely oversized in order to maintain the high thrust during the mission. Total propulsion system weight is estimated to be on the order of 100 kg. A summary of the all liquid propulsion system is shown in figure 24.

COMMUNICATIONS AND DATA HANDLING

The performance of the communications and data handling (C&DH) system depends primarily on the data rate and the transmitter power output. The data rate is fixed at 40 kilobits per second (kb/s) for the three core instruments, which yields about 2 Gb of data for each 15-h orbit. The data would be stored on a solid-state recorder and downlinked once per orbit. The recorder, with a minimum of 2.5 Gb capability, was selected based upon mass and power restrictions.

IMI SOLAR TERRESTRIAL PROBE
ALL LIQUID SPINNER SPACECRAFT

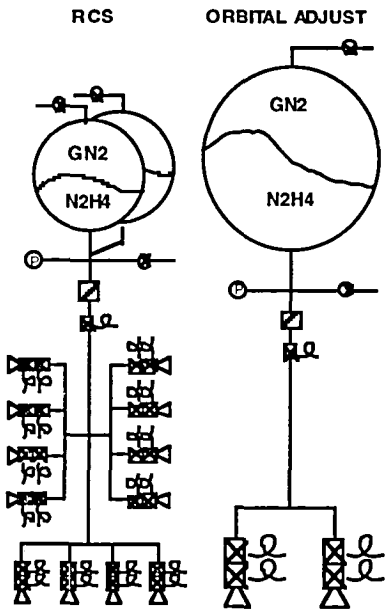

NUMBER	EQUIPMENT	WEIGHT (LB)	WEIGHT (KG)
5	FILL & DRAIN VALVES	2.50	1.14
1	O/A PROPELLANT TANK (22.14 ")	12.50	5.68
2	RCS PROPELLANT TANK (9.41 ")	6.50	2.95
2	PRESSURE TRANSDUCER	2.20	1.00
2	FILTER	2.00	0.91
2	ISOLATION VALVE	4.20	1.91
12	THRUSTERS (1 LBf)	9.60	4.36
2	THRUSTERS (15 LBf)	5.00	2.27
	MISCELLANEOUS (15%)	6.68	3.03
	TOTAL DRY WEIGHT	51.18	23.26
	PROPELLANT - USABLE	165.20	75.09
	RESIDUAL	3.37	1.53
	PRESSURANT	2.11	0.96
	TOTAL SUBSYSTEM WEIGHT	221.86	100.85

Figure 24. Schematic for propulsion system.

The downlink time and rate are dependent on antenna gain and transmitter power. With a spinning spacecraft, an omni-directional antenna with little or no gain is dictated. Transmitter output is limited by the dc power availability on the spacecraft. For the spacecraft, 10 W of radio frequency (RF) power was chosen as an acceptable compromise. A downlink rate of 1.5 mb/s was chosen as a value that will give acceptable transmission times at positive link margins. The 1.5-mb/s rate and 10 W of RF power will give positive link margins out to about four Earth radii with either the Deep Space Network (DSN) 26- or 34-m antennas, and a downlink time of about 24 min for one orbit of data. A minimum of 24 min of contact time with one of the DSN stations will be available on most of the IMI orbits.

Commands to the spacecraft will be at a much lower data rate and should be possible at any point in the orbit. Refinements of the communications and data handling system may be possible by varying data rate, transmitter power, or antenna type. These factors will be reexamined as the design of the system matures.

MASS PROPERTIES

The MI baseline system mass summary, shown in table 4, is a top-level summary of each spacecraft subsystem, the three core science instruments (table 2), and the propellant required for orbit boost and RCS. The current total launch mass is 413 kg with a 30-percent contingency on the spacecraft subsystems and science instrument masses. The launch margin of 68 kg is calculated using the estimated performance capability of the Conestoga 3632 to place 481 kg in the insertion orbit of 185 km by 7 R_E.

Table 4. Mass summary for the baseline mission.

	Baseline Core Instruments Full Size Electronics
Structures	60.4
Thermal Control System	4.8
Attitude Control System	22.0
Electrical Power System	24.5
Cabling/Harness Assembly	20.1
Communications and Data Handling	25.0
Propulsion System (dry)	23.3
Spacecraft Contingency (30 percent)	54.0
Spacecraft Dry Mass	234.1
Total Propellant	77.6
Science Instruments	78.0
SI Contingency (30 percent)	23.4
Total Launch Mass	413.1
Launch Margin (Conestoga)	67.7

☆ U.S. GOVERNMENT PRINTING OFFICE—1995—733-109/20082

REPORT DOCUMENTATION PAGE

Form Approved
OMB No. 0704-0188

1. AGENCY USE ONLY (Leave Blank)	2. REPORT DATE	3. REPORT TYPE AND DATES COVERED
	September 1995	Reference Publication

4. TITLE AND SUBTITLE

Magnetosphere Imager Science Definition Team Interim Report

5. FUNDING NUMBERS

6. AUTHOR(S)

T.P. Armstrong,* and C.L. Johnson

7. PERFORMING ORGANIZATION NAME(S) AND ADDRESS(ES)

George C. Marshall Space Flight Center
Marshall Space Flight Center, Alabama 35812

8. PERFORMING ORGANIZATON REPORT NUMBERS

M-794

9. SPONSORING/MONITORING AGENCY NAME(S) AND ADDRESS(ES)

National Aeronautics and Space Administration
Washington, DC 20546-0001

10. SPONSORING/MONITORING AGENCY REPORT NUMBER

NASA RP-1378

11. SUPPLEMENTARY NOTES

Prepared by Advanced Systems and Technology Office, Program Development
*University of Kansas

12a. DISTRIBUTION/AVAILABILITY STATEMENT

Unclassified-Unlimited

Subject Category 46

12b. DISTRIBUTION CODE

13. ABSTRACT *(Maximum 200 words)*

For three decades, magnetospheric field and plasma measurements have been made by diverse instruments flown on spacecraft in many different orbits, widely separated in space and time, and under various solar and magnetospheric conditions. Scientists have used this information to piece together an intricate, yet incomplete view of the magnetosphere. A simultaneous global view, using various light wavelengths and energetic neutral atoms, could reveal exciting new data and help explain complex magnetospheric processes, thus providing a clear picture of this region of space. This report documents the scientific rationale for such a magnetospheric imaging mission and provides a mission concept for its implementation.

14. SUBJECT TERMS

magnetosphere, geocorona, plasmasheet, spacecraft design

15. NUMBER OF PAGES

76

16. PRICE CODE

A05

17. SECURITY CLASSIFICATION	18. SECURITY CLASSIFICATION OF THIS PAGE	19. SECURITY CLASSIFICATION OF ABSTRACT	20. LIMITATION OF ABSTRACT
Unclassified	Unclassified	Unclassified	Unlimited

National Aeronautics and
Space Administration
Code JTT
Washington, DC
20546–0001

Official Business
Penalty for Private Use, $300

Postmaster: If Undeliverable (Section 158 Postal Manual), Do Not Return